
The University of Edinburgh

School of Engineering

Institute for Infrastructure and Environment

Academic Year 2018-2019

# Flame Propagation Between Flat Roofing and Photovoltaic Installations

**Student: Farah Binte Mohd Faudzi**

**Promoter: Prof. Grunde Jomaas**

Master thesis submitted in the Erasmus Mundus Study Programme

**International Master of Science in Fire Safety Engineering**

# DISCLAIMER

This thesis is submitted in partial fulfilment of the requirements for the degree of The International Master of Science in Fire Safety Engineering (IMFSE). This thesis has never been submitted for any degree or examination to any other University/programme. The author declares that this thesis is original work except where stated. This declaration constitutes an assertion that full and accurate references and citations have been included for all material, directly included and indirectly contributing to the thesis. The author gives permission to make this master thesis available for consultation and to copy parts of this master thesis for personal use. In the case of any other use, the limitations of the copyright have to be respected, in particular with regard to the obligation to state expressly the source when quoting results from this master thesis. The thesis supervisor must be informed when data or results are used.

*Read and approved.*

(17,197 words)

# ABSTRACT

An experimental investigation was carried out to provide a better understanding of the flame propagation between a flat roofing and photovoltaic installations in order to determine the influence of gap distance on the fire spread potential. Horizontal flame propagation along a combustible surface with a parallel incombustible surface above was studied experimentally for varying gap distances (10 cm to 25 cm). A 30 mm wide polymethylmethacrylate (PMMA) slab and a stainless-steel sheet was used as a surrogate for a combustible roofing material and an incombustible photovoltaic (PV) module, respectively. The advancement of the flame front and mass loss rate was measured, and so was temperatures of the PMMA slab, gas phase temperatures in the gap and radiative heat flux. For tests with gap distance of more than 20 cm, constant flame spread rates were achieved and the burning velocity of 0.15 – 0.20 mm/s is comparable to a free burning scenario. However, for smaller gap distances, the flame spread had a growing phase followed by rapid acceleration once the flames impinged the modules. A resultant flame spread rate of 2 mm/s was recorded for all gap distances smaller than this critical value. Thus, the experimental investigation revealed the significance of a critical gap distance for PV installations above which the horizontal flame spread hazard could be minimised. Similar experiments carried out with actual PV modules concur with the trends observed in the experimental set-up. The findings can form a preliminary understanding of the impact of a PV panels on flames propagating along the roof.

# ACKNOWLEDGEMENTS

*"You'll never walk alone."*[1]

And I never did for I had the blessing of being around the following amazing people that not only made this thesis possible but also the whole IMFSE journey one I will treasure for life.

First and foremost, a heartfelt thanks to Prof. Grunde Jomaas who was not only my supervisor who continually challenged me but also a mentor who believed in me even when I was on the brink of giving up. A shout-out to my partner in ~~crime~~ the fire laboratory, Jens Steemann Kristensen, who despite having a questionable playlist, was an outstanding inspiration and kept me going throughout the long tiring days (and nights) in DTU fire lab. Kudos also to the team in DTU for all your support (and yes, Jonas, you made it to my thesis!).

At the same time, I am also blessed with a great support system back in Edinburgh. Thanks to Dr Stephen Welch for his enthusiastic discussions on my work, Dr Richard Emberley for taking time to discuss the project during your visit here, to Zak, Ben, and Simon for sharing your thoughts on the project, to Martina for her never-ending encouragement and finally to my "BFF" Arjan for making sure I am taking enough breaks from my nest in the KB library.

To my IMFSE family. The "bois" in Edinburgh who have showered me with extremely tough love (Balsa, Jaime, Gerard, Lei and Dheeraj), Tanveer, Ayyappa, Giorgos, (where's) Yalong, Ines, Kristi, Miqdad, Bogdan, the kangaroo to my koala, Andrei and most lovingly, my sisters from another mother, Silvia and Kate. May the friendships form last a lifetime.

To my real family and friends back home in the tiny island of Singapore with a big heart, no matter the distance, I can always feel your love and support. Only you would understand what this means to me and I hope to make you proud…

From the words of Moana:

"*If the wind in my sail on the sea stays behind me*
*One day I'll know, how far I'll go."*

So, thanks for being the wind in my sail, for always having my back. With you always behind me, there's just no telling how far I'll go… For now, let's see where THIS goes. As JSK always says *"Are you ready to save the world?"*

[1] Disclaimer: Author is not a Liverpool fan…

# CONTENTS

**Disclaimer** ..... **i**
**Abstract** ..... **iii**
**Acknowledgements** ..... **v**
**List of Figures** ..... **ix**
**List of Tables** ..... **x**
**1 Introduction** ..... **1**
1.1 Background ..... 1
1.2 Applications of Flame Spread Theories ..... 4
1.3 Effect of Imposed Heat Flux Caused by The Panel ..... 6
1.4 Aims and Objectives ..... 11
**2 Methodology** ..... **13**
2.1 Experimental set-up ..... 13
2.3 Experimental Procedure ..... 18
2.4 Video Analysis Method ..... 19
**3 Experimental Results and Discussion** ..... **21**
3.1 Visual observations ..... 21
3.2 Flame Spread Rate, Flame Height and Pyrolysis Zone ..... 24
3.3 Mass Loss Rate Measurements ..... 34
3.4 Surface Temperatures Measurements ..... 38
3.5 Gas-phase Temperature Measurements ..... 42
3.6 Measurements of Radiant Heat Flux ..... 45
3.7 Energy Balance for Flame Spread ..... 48
3.8 Experiments with Actual PV Panels ..... 53
**4 Conclusion** ..... **59**
4.1 Future Work ..... 61
**5 References** ..... **63**
**Appendix 1: Determining Sample Dimensions** ..... **67**
**Appendix 2: Full Experimental Matrix** ..... **69**
**Appendix 3: PMMA Temperatures (Raw Data)** ..... **71**
**Appendix 4: Comparison with PV Panels** ..... **75**

# LIST OF FIGURES

Figure 1 Illustration of the heat transfer mechanisms involved in flame spread .....5
Figure 2 Illustration of heat transfer mechanisms involved in flame spread due to the presence of the panel .....7
Figure 3 Impact of flame height for open burning (top), $L_f < H$ (middle) and $L_f < H$ (bottom) .....8
Figure 4 Gas temperatures near the panel based on ceiling jet correlations for a 2.5kW fire for different H .....9
Figure 5 Illustration of factors determining rate of burning..... 10
Figure 6 Simplification of the orientation of PV panels ..... 13
Figure 7 Schematic of the experimental set-up (all dimensions in mm)..... 14
Figure 8 Set-up for the PMMA sample ..... 16
Figure 9 Final Set-up ..... 17
Figure 10 Simultaneous linear ignition along ceramic paper (left) eventually ignite the PMMA (right)..... 19
Figure 11 Progress of the experiment was monitored ..... 19
Figure 12 Reference points for discussion ..... 19
Figure 13 Example of how record of flame front is monitored ..... 20
Figure 14 Example of how the different measurements were obtained ..... 20
Figure 15 Observations of flames for Test 1-3 (see Table 2 shows the experimental matrix for the tests that would be analysed in this study. ..... 22
Figure 16 Flame observations for Test 4-6 (H = 17 cm, H = 15 cm and H = 10 cm)..... 23
Figure 17 Surface bubbling in the growth phase (left) and the accelerated phase (right)..... 23
Figure 18 Conceptual diagram of observations..... 24
Figure 19 Progress of the flame front over time for various panel heights..... 25
Figure 20 Accelerated flame spread at the onset of deflection of flames under the plate .... 26
Figure 21 Length of Pyrolysis Zone for Test 1-3 (no panel; H = 25 cm; H = 20 cm) ..... 28
Figure 22 Flame characteristics over time for Test 4 (H = 17 cm)..... 30
Figure 23 Flame Characteristics over time for Test 5 (H = 15 cm) ..... 31
Figure 24 Flame Characteristics over time for Test 5 (H = 10 cm) ..... 31
Figure 25 Thermocouple records for flame spread (Test 5: H = 15 cm)..... 32
Figure 26 Comparison of image processing and visual observation data for Test 6 (H = 10 cm) ..... 33

Figure 27 Mass readings versus time ..... 34
Figure 28 Mass Loss Rate for Test 4-6 (H = 17 cm; H = 15 cm; H = 10 cm) ..... 36
Figure 29 Temperature profiles of the PMMA sample ..... 39
Figure 30 Limitations of temperature measurements ..... 42
Figure 31 Gas temperatures in the gap between the panel and sample for test 2 and 3 ..... 43
Figure 32 Gas temperature profiles for Test 6 (H = 10 cm) ..... 44
Figure 33 Comparison of gas temperatures at midplane of the gap ..... 45
Figure 34 Radiative heat flux over distance away from the flame front ..... 47
Figure 35 Diagram for heat balance calculations ..... 48
Figure 36 Distribution of heat fluxes ahead of the flame ..... 51
Figure 37 Conceptual energy balance diagram for the system ..... 52
Figure 38 Modification to set-up for tests with PV panels ..... 53
Figure 39 Similar observations for H = 20 cm when flames reach mid-point of the sample. 54
Figure 40 Similar observations for H = 15 cm & H = 17 cm ..... 55
Figure 41 Debris from combustible panel on the sample set-up ..... 56
Figure 42 PV panels after the experiment ..... 57
Figure 43 Progress of the flame front over time ..... 58
Figure 44 Flame propagation over time for 300 mm length ..... 67
Figure 45 Mass over time for 300 mm length ..... 68
Figure 46 Mass loss readings for PV surrogate and PV panel ..... 75
Figure 47 Gas temperature comparison between PV surrogate and PV panel (top: H = 20 cm; middle: H = 17 cm; bottom: H = 15 cm) ..... 76

# LIST OF TABLES

Table 1 Factors affecting rate of flame spread over combustible solids [23] ..... 6
Table 2 Experimental matrix ..... 18
Table 3 Flame spread rates of test 1-3 ..... 28
Table 4 Mass Loss Rate for Test 1&3 (No Panel; H = 20 cm) ..... 35
Table 5 Verification of mass loss rate data ..... 37
Table 6 Comparison of energy required for ignition and heat transfer to the sample ..... 51

# 1 INTRODUCTION

## 1.1 BACKGROUND

Solar photovoltaic (PV) power generation has increased exponentially over the last 10 years from 9.2 GW in 2007 to 404.5 GW in 2017 [1]. This trend is driven by an increased demand for renewable and sustainable energy sources as well as the emergence of innovative technologies which reduce the costs while improving the efficiency of these systems [2]. Being a financially viable alternative energy source, rooftop PV power systems enable companies to reduce their dependence on the local grid and manage their energy expenses with prices of commercially installed systems declining by 73% since 2010. These on-site solar installations are particularly effective for buildings with large footprints and flat roofs. In the US, rooftop systems constitute a large majority of corporate solar installations making up 70% in terms of total capacity and 89% of all corporate installations [3]. The existing extensive installations of PV installations on roofs coupled with the potential future growth would result in rooftop PV systems being commonplace in most buildings with flat roof constructions.

However, fire incidents occurring globally involving rooftop PV systems raise concerns regarding the impact of such systems on the inherent fire risks. These include an office in Wisconsin installed with a 70 kW PV system on the roof where 4,000 $m^2$ of the building was destroyed in a fire with a partial roof collapse in 2013 [4]. In Germany, fire incidents in a warehouse in Walldorf in 2014 and in a workshop in Nordeney in 2013 both with rooftop PV installations resulted in significant financial losses [5]. In Italy, the Italian National Firefighters Brigade has responded to 1600 PV-related fire incidents out of 590,000 PV plant installations by 2014 [6]. These fire incidents not only emphasise the contribution of rooftop PV installations to building fire risks but also highlights the potential damage that could result from such fires.

The extent of damage on the building can be correlated to the extent of fire spread along the roof equipped with PV installations. Fire investigations on past incidents imply that installation of PV systems leads to changed conditions for fire propagation and fire spread. Typically, in industrial buildings and logistic warehouses, roofs are constructed from materials with poor fire performance such as polyurethane sandwich panels. Although they are good thermal insulators, they are easily ignitable and facilitate fire spread [6]. Fiorentini et al. cited findings from a fire investigation of a 1000 $m^2$ warehouse equipped with a PV plant where sustained fire was observed due to the substantial amount of fire load provided by the existing thermally

insulated roof made of thick combustible foam layers [7]. In a 2013 fire at the Dietz and Watson Factory in Delanco, New Jersey, unprotected combustible roofing equipped with 1.6 MW of PV installations was said to allow the fire to spread and provided significant fuel source to the fire [8]. Regulations have been placed in certain countries to address this by focussing on the flammability characteristic of the roof and PV panels individually. In Italy, requirements to mitigate the risks include t conducting a risk assessment considering the class of external fire protection of roofs and roof coverings performed according to CEN/TS 1187:2012 as well as class of reaction to fire of the PV panel. PV installations are also deemed acceptable if installed on incombustible structures and roofing elements [6]. However, the risks involving rooftop PV installations are not only limited to systems with unprotected or combustible roofing materials. A fire caused by a PV system in Goch in 2012 revealed that a typical "hard roofing" with sanded bitumen roof sheeting, which normally acts as protection against radiant heat and flying sparks, was not able to provide effective protection in combination with an installed PV system leading to a major fire. [5]. From the latter incident, it can be concluded that the flammability characteristic of the PV panels and roof construction individually is not the only factor determining the fire behaviour on such rooftop configurations. As such, the relevance of the study on the interaction between the PV panels and roof construction is necessary in order to understand its influence on fire propagation along the roof and the resultant fire hazard it poses.

The gap between the PV panels and the roof surface have been shown to contribute to conditions that could facilitate flame propagation compared to a free burning scenario. For example, experiments carried out by Kristensen et. al. to characterise the fire risks of PV panels on typical roof constructions shows that the presence of PV panels alters the fire behaviour on roofs by introducing a significant increase in heat flux directed back to the existing roof [9]. In addition, Backstrom's experimental work with Underwriters Laboratories also shows that the presence of rack mounted PV panel has an adverse effect on the fire performance of the roof regardless of the fire rating of the roof or the PV panel itself [10]. His experiments also concur with Kristensen's work that higher temperatures and heat fluxes were found on the roof surface due to the presence of the PV panels in the event of a fire [11]. However, these studies were carried out based on a fixed stationary fire source and does not account for how the increased heat flux and temperatures would affect flame propagation and potential fire growth. Thus, existing studies should be expanded to analyse how these effects would affect the fire spread on such roof constructions.

An enhanced knowledge on the mechanisms by which fires spread within the gap between the roof and the panel can help in the prevention and control of such fires. Standard tests such as Spread of Flame Test as described by UL790 study the impact of fire spread due to the presence of the PV panel based on measurements of spread distance within a specified test duration [12]. However, such metrices are mainly used as a pass/fail criterion on the roofing combustibility and does not quantify the increased risk due to characteristics of the gap that could influence fire spread. An analysis on how the flame spread characteristics are driven by the increased heat fluxes as well as the increased temperatures both within the gap and the surfaces is required. Separation gap between the roof and PV panel have been identified as a potential parameter that could affect fire spread [13]. Given the variety of materials used for both PV and roof construction, decoupling of the material properties and its role in fire spread would be able to reveal the fundamental processes that drive fire spread along the gap. An analysis of the influence of the gap between the incident non-combustible surface (i.e. PV panel[2]) and the combustible surface (i.e. roof surface) can provide insights on its role on the extent and severity of fire spread on the roof.

Gap distance could possibly be used as a mitigating measure to reduce the severity of fire spread on roofs installed with PV panels. Typical gap height for PV installations on roofs are mainly driven by factors such as architectural interests, structural considerations and wind load. Seismic considerations for PV installations have restricted the gap height to less than 36 inches (90 cm) or half of the smallest plan dimension supporting the array [8]. Gap distances are also limited in order to prevent excessive uplift in wind conditions [14]. These considerations tend to limit the gap distances between PV installations and the roof. However, increasing the gap distance have been shown to reduce the effects of higher temperatures and heat flux received due to the presence of the panel in the event of a fire [12]. Experiments carried out by Hong on fire spread on roofing membrane in the presence of PV panels observed that fire spread and heat release rate of the fire was lower when the fire was further from the underside of the PV panel [15]. With these competing interests driving the design of PV installations on roofs, it is critical that fire safety considerations are not neglected when establishing the gap height of PV installations in mitigating the risk of fire spread from such roofs while a fulfilling other design criterion in order to obtain an economical solution.

[2] The PV panels are considered to have limited combustibility which is insignificant compared to the propagation of fire on the combustible roof surface ([9], [42]).

From the above discussion, fire incidents have highlighted that there is an increased risk of fire spread due to PV installations on roof constructions. Although this could be attributed to the material combustibility, the gap between the PV installations can also play a significant role in facilitating fire spread due to the changed dynamics of the fire within the gap. Therefore, an understanding of the interactions between the two surfaces i.e. the PV panel and the roof surface in a fire situation would allow for characterisation of the fire spread within the gap and establish an understanding on how gap distances would affect the potential for hazardous fire spread.

## 1.2 APPLICATIONS OF FLAME SPREAD THEORIES

The fire growth rate on a roof with PV installations depends on how rapidly a flame can spread from the ignition point to involve an increasing area of the roof. Flame spread can be regarded as the propagation of an ignition front involving heat transfer processes in which the flame front acts as both a heat source to increase the temperature of the fuel to ignition temperature as well as a pilot ignition source to sustain flaming [16]. Heat from the flame is transferred to the unburned fuel bed ahead of the flame until it vaporises and then reacts with the oxygen entrained into the flame. The energy released is then transferred to the unburned fuel bed ahead of it. As such, an energy cycle is created which is necessary to maintain the fire-spread process [17].

Based on the application of energy conservation principle, Williams termed the following relationship as the fundamental equation of fire spread [18]:

$$\rho v \Delta h = \dot{q}^{"} \qquad (1)$$

where $\dot{q}^{"}$ is the rate of heat transfer across the surface (W/m$^2$), $\rho$ is the density of the fuel (kg/m$^3$), $v$ is the rate of spread (m/s) and $\Delta h$ is the change in enthalpy (per unit mass of fuel) between the fuel at its ignition temperature and the virgin fuel (J/kg). From this equation, it is essential to establish $\dot{q}^{"}$ by identifying the different modes of heat transfer across the surface of fire inception in describing fire spread. The heat transfer from the flaming region of the fuel to the virgin fuel is the central process in fire spread along a solid fuel surface [19]. Quintiere proposed a similar relationship for the speed of an idealised laminar premixed flame where $\dot{q}^{"}$ relates to the chemical energy release rate instead of the rate of heat transfer [20]. This difference highlights the complexity of flame spread analysis as the accurate description of the flame spread mechanisms does not only include the heat transfer processes but also the chemical processes such as vaporization of the fuel ahead of the flame, the flammable mixture formed by the vaporised fuel and the oxidiser and the propagation of the

flame along this mixture. Although ignition temperature controlled by the chemical kinetics of pyrolysis and density of fuel area also factors affecting the flame spread rate, the influence of heat transfer would be more critical in our analysis to study the changed dynamics due to the presence of the PV panel. The Damkohler number (ratio of flow time to chemical time) is expected to be large due to low flow velocities [21]. In such cases, the flame spread process is controlled by heat transfer mechanisms from the flame to the fuel. This study will focus primarily on the heat transfer mechanisms in the flame spread process across a surface and how it is affected due to the presence of the PV installation. In particular, the study will elaborate on the effect of different gap distances on the flame spread behaviour.

The three primary heat transfer mechanisms occurring are radiation from the flame, conduction/convection through the gas ahead of the flame and conduction through the solid fuel [19]. Ray et al. constructed the following energy balances to analyse the different mechanisms of heat transfer from the flame to the virgin material ahead:

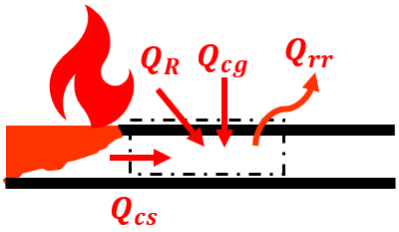


Net outward heat flow, $Q$ = heat conducted through the solid, $Q_{cs}$
+ heat conducted through the gas, $Q_{cg}$
+ heat transferred by radiation from the flame, $Q_R$
– heat reradiated at the fuel surface, $Q_{rr}$

*Figure 1 Illustration of the heat transfer mechanisms involved in flame spread*

While the different heat transfer modes are involved to some extent, an understanding on the dominant mechanism will enable the development of simplified characterisation of the fire spread process together with an understanding on how various factors would affect flame spread in our scenario. Friedman identified the several factors affecting the flame spread rate over combustible solids (see Table 1). The relevant factors that are pertinent to the heat transfer mechanisms for this study will be discussed.

As the context of this study is related to flat roof constructions, flame spread along a horizontal surface orientation will be considered. Although roofs are exposed to wind effects that could affect flame propagation, this study will focus on horizontal flame propagation along a surface with the absence of an external flow in order to neglect the effects of wind. Nevertheless, in a relatively quiescent atmosphere, a naturally induced counter-current flow

is generated due to the dynamics of the flame which causes a flow of air that opposes the direction of spread. Such a scenario is commonly referred to as opposed flame spread. It has been studied that similar to downward flame spread, constant spread rates will be achieved in horizontal flame spread with the absence of external air flow [22]. Based on these criteria, horizontal opposed flow flame spread in a free burning scenario is studied as the baseline case.

*Table 1 Factors affecting rate of flame spread over combustible solids* [23]

| **Material Factors** | | **Environmental factors** |
|---|---|---|
| Chemical | Physical | |
| • Composition of fuel<br>• Presence of retardants | • Initial temperature<br>• Surface orientation<br>• Direction of propagation<br>• Thickness<br>• Thermal capacity<br>• Thermal conductivity<br>• Density<br>• Geometry<br>• Continuity | • Composition of atmosphere<br>• Pressure of atmosphere<br>• Temperature<br>• Imposed heat flux<br>• Air velocity |

## 1.3 EFFECT OF IMPOSED HEAT FLUX CAUSED BY THE PANEL

The key parameter that has been identified in previous experiments with PV panels is the imposed heat flux due to the presence of PV panels which caused a significant increase of radiative heat flux due to re-radiation from the fire by the PV panels (compared to the scenario without the PV panel) [9]. The heat transfer process illustrated for a free burning scenario in Figure 1was modified to include this re-radiation as shown in Figure 2.

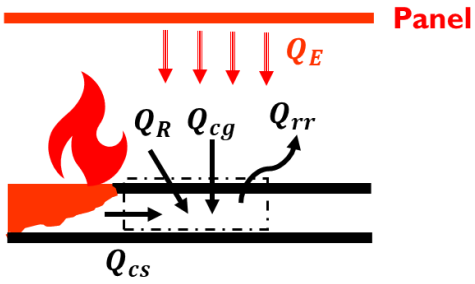


Net outward heat flow, $Q$ = heat conducted through the solid, $Q_{cs}$
+ heat conducted through the gas, $Q_{cg}$
+ heat transferred by radiation from the flame, $Q_R$
+ external heat flux, $Q_E$
– heat reradiated at the fuel surface, $Q_{rr}$

*Figure 2 Illustration of heat transfer mechanisms involved in flame spread due to the presence of the panel*

An imposed radiative heat flux will cause an increase in the rate of flame spread primarily due to pre-heating the fuel ahead of the flame front and thus, increasing the temperature of the unaffected fuel. As such less heat is needed to increase the temperature of the unaffected fuel to ignition temperature [22]. Due to the effect of $Q_E$, this study will aim to investigate its effect in relation to the gap distance in order to form a correlation between flame spread and the gap distance.

In a free burning scenario, radiative heat flux from the flames have been identified as the dominant mechanism of heat transfer for large scale fires. Ray et. al. concluded that for large fires, radiative heat transfer from the flames plays a significant role in horizontal flame spread as a fuel preheating mechanism affecting the temperature of fuel over an extended length [19]. Williams proposed a rough equation to describe radiation heat transfer in horizontal flame spread as such [18]:

$$q_f = \in_f \sigma_b T_f^4 L_f sin\theta_f / \delta \qquad (2)$$

where the flame height $L_f$(m), its emissivity $\in_f$, flame temperature $T_f$ and its average angle with respect to the fuel surface $\theta_f$ would contribute to the radiant heat transport (Stefen-Boltzmann constant: $\sigma_b$). For a thermally thin fuel, $\delta$ could be correlated to the thickness of the fuel. From equation (2), it can be deduced that flame height would have an impact on the radiative heat transfer in a free burning scenario. With the introduction of the panel, additional heat transfer mechanisms are imposed on the fuel as illustrated in Figure 3 depending on the gap height, H, with respect to the flame height.

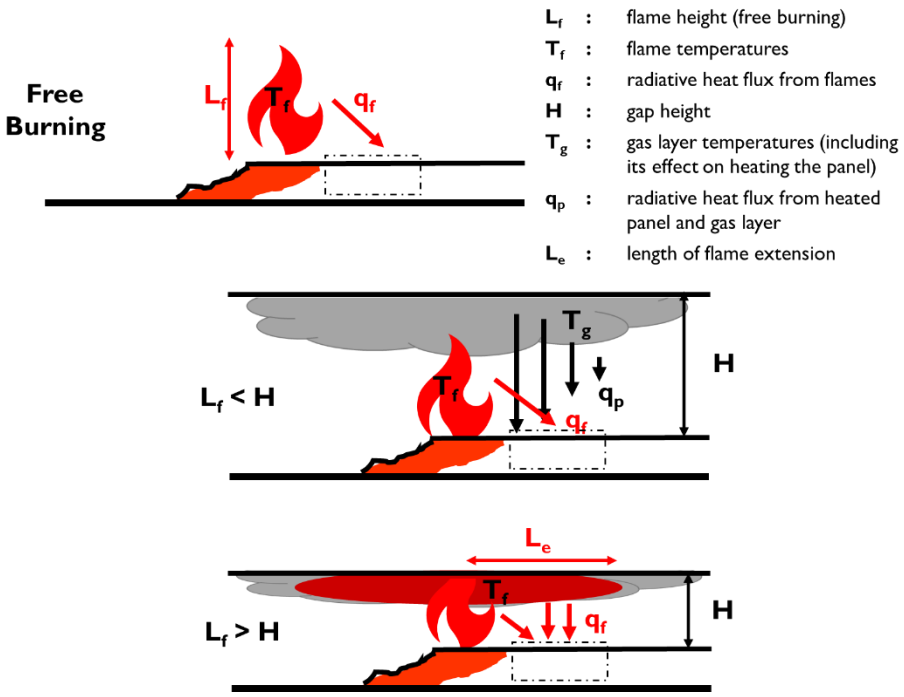


*Figure 3 Impact of flame height for open burning (top), $L_f < H$ (middle) and $L_f < H$ (bottom)*

In the scenario where H > $L_f$, the influence of the panel on fire spread is dependent on the magnitude of the imposed heat flux from the panel. The imposed heat flux arises from the fire plume rising above the burning fuel and impinging on the panel which form a ceiling jet under the panel surface that moves radially under the panel to other areas further from the fire. Ceiling jet refers to the relatively rapid gas flow in a layer beneath the ceiling surface that is driven by the buoyancy of the hot combustion products from the fire plume [24]. The presence of the panel is analogous to an unconfined ceiling. As such, Alpert's ceiling jet correlation is applicable to provide an approximation of the temperature distribution within the gas layer, $T_g$. These correlations relate the maximum ceiling jet excess temperatures near the panel with the following parameters: i) the total heat release rate (HRR), ii) the radial position from the axis of the fire plume, iii) the gap distance. Although the quantification of the gas temperatures based on the correlations are not applicable to this study, these correlations reveal the temperature profiles of the gas layer formed above the burning surface which can act as an indication on the intensity of the radiant heat flux caused by the gas layer on the burning surface below. The gas layer also heats up the panel by convection (due to the rapid gas flow beneath the ceiling) and radiation which causes the panel to radiate heat itself back to the unburnt surfaces. In addition, the panel also heats up due to direct radiation from the flames. Deducing from the temperature profiles obtained from these correlations shown in Figure 4, the imposed radiative heat flux from the gas layer and the panel would be higher nearer to the fire and decrease radially away from the fire. The latter effect is

exponential as the radiation is in the function of temperature to the power of four. Decreasing the height of the panel will extend the ceiling jet and intensify the radiative flux to the burning surface as the gas temperatures would be higher in this configuration (compared to free burning). As such, the flame spread will increase due to the increasing pre-heated length of the fuel prior to flame arrival.

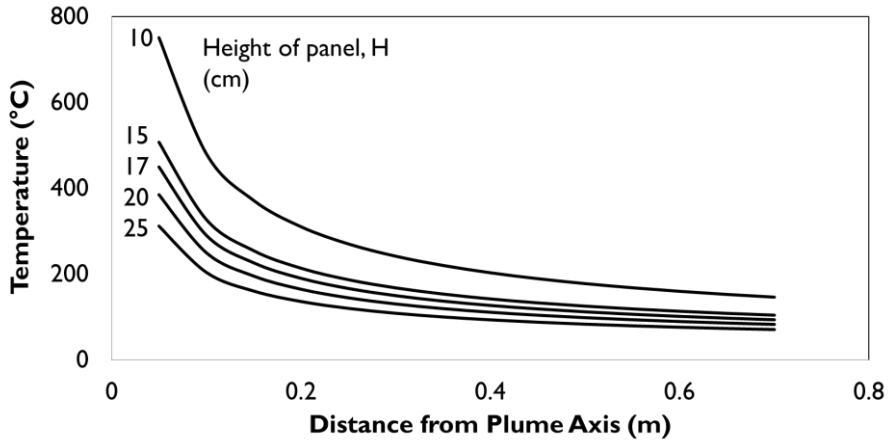


*Figure 4 Gas temperatures near the panel based on ceiling jet correlations for a 2.5kW fire for different H*

In the scenario where $H < L_f$, the free burning height of the flames exceed the height of the gap and the fire impinges on the panel. As result, the flame is deflected horizontally and becomes part of the ceiling jet underneath the panel. Horizontal flames radiate more heat to facilitate fire spread than vertical flames due to a higher view factor between the flames and the fuel surface. In addition, horizontal flames also radiate more heat compared to the gas layer and the heated panel due to the inherent high flame temperatures. In a flame impingement scenario, the behaviour of the flame spread is akin to a concurrent flow flame spread as the flame is pushed forward ahead of the pyrolysis region. As such the transfer of heat from the flames to the virgin material is facilitated. It can be expected that the effect of the latter on the flame spread speed would be similar to an upward flame spread scenario for which upward spread is accelerative for thick materials while a constant but rapid rate of spread can be achieved for materials with finite thickness [18]. The extent of the horizontal flame deflection has been found to be related to the flame height in the absence of the ceiling. Babrauskas found that the mean radius of the horizontal flame is 1.5 times the "cut-off height" i.e. $L_f$ (free burning) – H [16]. The flame extension determines the pre-heating length upstream from the flame front. Thus, flame spread characteristics for this scenario would drastically differ from the free-burning and the first scenario.

An indirect effect of an imposed heat flux would be its contribution towards the burning rate of the fire. The presence of the panel provides a thermal feedback through the hot gas/flame

layer and the heated panel itself towards the burning surfaces by radiation. As such, the rate of burning is enhanced. The following equation for rate of burning presents the effect of the panel as an external heat flux imposed on the burning area.

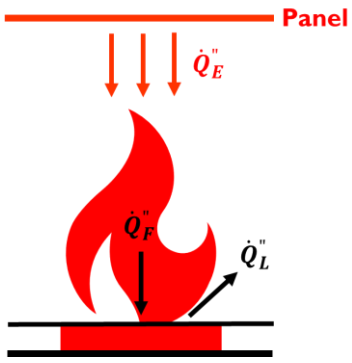


*Figure 5 Illustration of factors determining rate of burning*

$$\dot{m}'' = \frac{\dot{Q}''_F + \dot{Q}''_E - \dot{Q}''_L}{L_V} \quad (3)$$

where $\dot{m}''$ = rate of burning expressed as a mass flux (kg/m²s)
$\dot{Q}''_F$ = heat transferred back to the fuel surface from the flames (kW/m²)
$\dot{Q}''_L$ = heat losses as a heat flux from the surface (kW/m²)
$\dot{Q}''_E$ = external heat flux imposed on the surface (kW/m²)
$L_V$ = effective heat of vaporisation of the fuel (kJ/kg)

The increased rate of burning contributes to the flame spread through its impact on the fire size and enhance the heat feedback from the flame to the upstream virgin surfaces [23]. The rate of burning contributes to the fire size or heat release rate through the following equation:

$$\dot{Q} = \chi \dot{m} \Delta H_c = \chi \dot{m}'' A \Delta H_c \quad (4)$$

where $\dot{Q}$ = rate of heat release (kW)
$A$ = surface area of the fuel (m²)
$\Delta H_c$ = heat of combustion of the fuel (kJ/kg)
$\chi$ = combustion efficiency
$\dot{m}$ = mass loss rate of fuel (kg/s)

Other than the mass burning rate, the surface area of the fuel also contributes to the rate of heat release. Thomas argues that the rate of fire development is influenced more by the increase in the area of burning than the increase of the rate of burning [25]. Thus, in this study, this effect will be investigated but will not be studied in detail.

## 1.4 AIMS AND OBJECTIVES

Based on the above discussion, the objective of this thesis is to analyse the propagation of fire along a horizontal combustible surface given the presence of a non-combustible surface above it. An experimental set-up is proposed as a preliminary study to characterise the fire dynamics and fire spread behaviour with respect to the gap between two surfaces. The gap distance is varied to understand the influence of this installation parameter on flame spread propagation on roofs with PV installations. Through this study, the risk of hazardous fire spread involving PV panel on the roofs could be better understood. Analysis on how gap distances impact this phenomenon will also reveal potential mitigation methods that could be adopted in regulations besides the currently existing requirements for material combustibility for PV installations on flat roofs.

# 2 METHODOLOGY

## 2.1 EXPERIMENTAL SET-UP

An experimental set-up was designed to investigate the effects of the panel on flame spread propagation. As PV arrays are often installed in various height and inclinations from the roof surface, a horizontal panel will be considered in the experimental set-up as a representative orientation. An inclined panel can be discretised as a series of horizontal surfaces as shown in Figure 6. Thus, the set-up will consider the flame spread along a horizontal surface with the presence of a horizontal parallel panel above it.

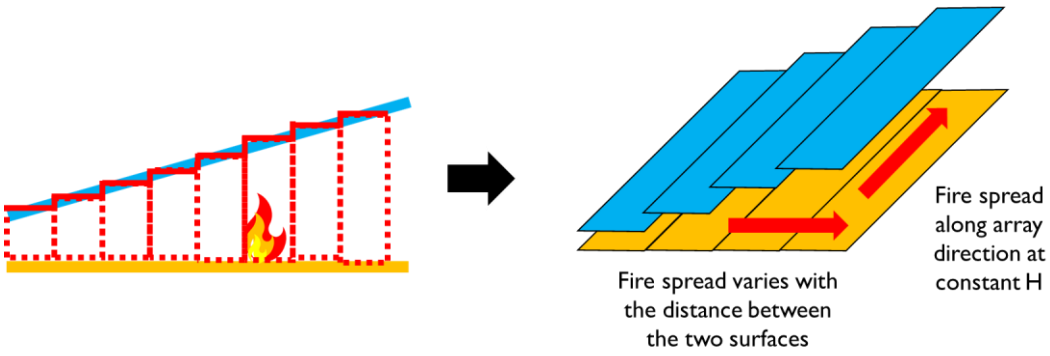


*Figure 6 Simplification of the orientation of PV panels*

Figure 7 shows a schematic of the experimental set-up designed for this study.

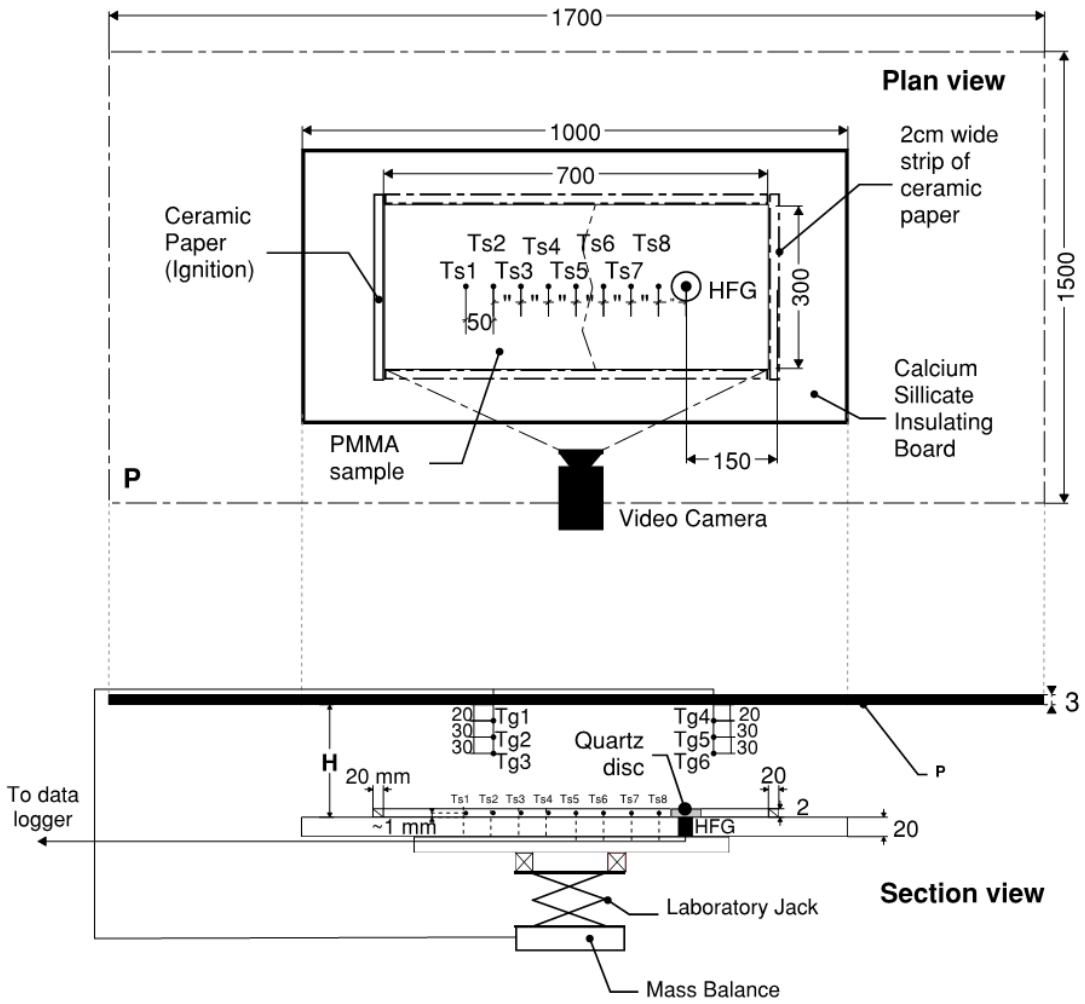


*Figure 7 Schematic of the experimental set-up (all dimensions in mm)*

Material P is the horizontal surface representing the PV panel. A 3 mm stainless steel sheet was used as a surrogate material for the PV panel. Stainless steel is used as a non-combustible board to isolate the influence of the installed panel on the thermal impact to the roofing assembly as it will not contribute to the fire load. The bottom surface is also painted black to resemble a blackbody. The stainless-steel sheet is sized to 1.7 m x 1.5 m to resemble the typical size of a PV panel. Actual PV panels would also be used as material P to investigate if similar results could be obtained[3]. Panels are supported on an aluminium frame structure.

For the fuel sample, polymethyl methacrylate (PMMA) is used as a surrogate material for the combustible roofing material. Extruded PMMA is used as a surrogate material for combustible roofing membranes as its properties are also well known and burning mechanisms are orderly and reproducible ([19],[26]). As flame spread involves heat transfer processes that includes

[3] Dimensions of Material P will differ for the actual PV module used for this study. See Figure 38.

heat transfer by conduction from the surface to the interior of the fuel, thickness of the PMMA slab would affect flame spread. As the burning characteristics of the combustible material itself is not the focus of the study, the use of a thermally thick materials would compound the study. Alternatively, a thermally thin fuel can be treated by the 'lumped thermal capacity model' whereby there is no temperature gradient across the front and back of the surfaces and the rate of spread will be inversely proportional to the thickness of the material [16]. Thus, 2 mm thick PMMA sheets were used in order to characterise a thermally thin material [27]. The PMMA sample was cut to a size of 300 mm wide and 700 mm length by a laser cutting machine. As width effects has been investigated to influence horizontal flame spread [28], 300 mm has been selected as the sample width such that it is comparable to other horizontal flame spread experiments for PMMA to represent large scale fires [19]. 700 mm length is used to capture changes in fire spread behaviour between each test sufficiently. Preliminary tests[4] using shorter samples of 300mm length with no panel and with a panel 15 cm above the sample reveal that the length of the sample must be increased in order to capture the differences in flame spread behaviour sufficiently. 20 mm strips of ceramic paper are also used as inhibitor along the edges of the PMMA slab to prevent preferential flame spread along the edges. Data scatter could also be reduced by not exposing the edges [29]. The bottom surface of the PMMA sample sheet is insulated with a non-combustible calcium silicate insulating board.

Temperatures in the PMMA are measured by Type K 14-gauge thermocouples. Based on the assumption of the thermally thin fuel treated as the 'lumped thermal capacity model', the thermocouples to measure the surface temperatures are embedded into the PMMA slab to represent the temperature of the surface. The thermocouples are pulled through the insulating board such that the tip is protruding 1 mm from the board. The tips are then heated with a burner to elevated temperatures (>400°C i.e. significantly above the melting point of PMMA(~160°C)[16]) to soften the PMMA slab when the slab is placed on the heated thermocouple tip. This allows the thermocouple to be embedded into the thickness of the PMMA. As the thermocouple cools, the tip remains bonded to the PMMA sheet. Due to the method adopted, a thicker thermocouple tip would better facilitate the installation of thermocouple into the PMMA sample as it can withstand the load without bending when the sample is placed on the board with pressure. Eight (8) thermocouples would be embedded along the centreline of the PMMA board at 50 mm apart through this procedure. Due to the propensity for the PMMA to soften and warp at elevated temperatures when in contact with

[4] See Appendix 1

the heated thermocouple tips, the PMMA sample is laser cut into two pieces so that this process is manageable without deformation of the PMMA to ensure good contact between the thermocouples and the sample.

A water-cooled heat flux gauge (Hukseflux SBG01-020) is used to measure the incident radiative heat flux as the flame approaches from the ignition end. A working range of 20 kW/m$^2$ was selected since the average of the maximum radiative heat flux from each test ranges from 0.0035 kW/m$^2$ to 50kW/m$^2$. The heat flux gauge is placed in the centreline of the sample by laser cutting a hole through the sample 55 mm from the ignition end. This arrangement may disturb the flame spread process, but preliminary experiments [5] demonstrated that the width of the sample is sufficient whereby there is negligible influence in terms of flame spread velocity and mass loss rate when the flame front splits around the heat flux gauge. A quartz disc is placed flushed with the sample above the sensing element to protect it from direct flame exposure.

These components form the set-up for the PMMA sample as shown in Figure 8.

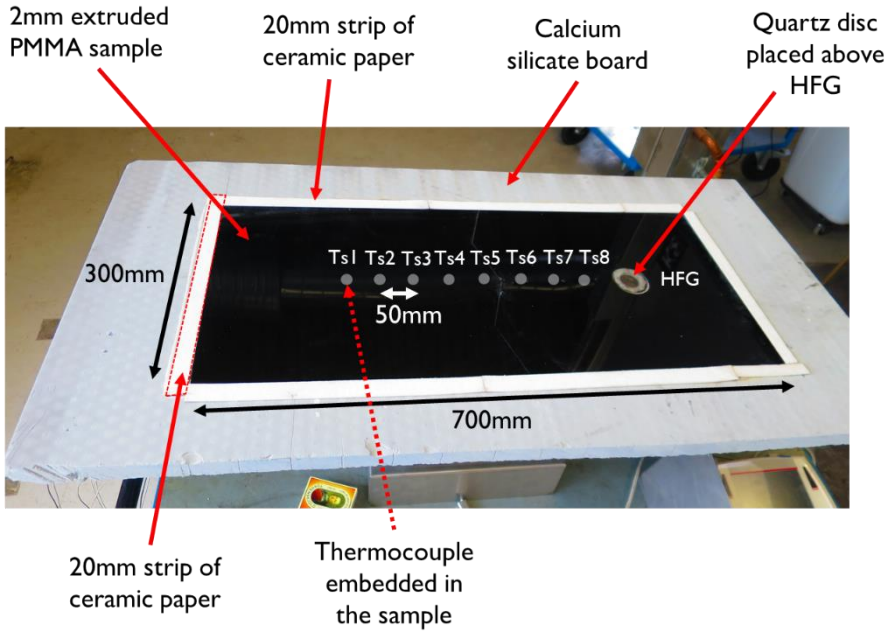


*Figure 8 Set-up for the PMMA sample*

Temperatures within the gap are measured at two points along the gap at 3 different heights (20 mm, 50 mm and 70 mm from the top panel surface) by Type K 24-gauge thermocouples. These measurements would provide the temperature profiles within the gas phase of the flame spread process within the gap between the two horizontal surfaces.

[5] See Appendix I

The PMMA sample set-up is mounted on a laboratory jack that could vary the distance between the PMMA surface and the panel surface. The gap heights between the sample and the panel are selected based on Backstrom's consultation with solar industry representatives which established distances of 2.5 inch (6.35 cm) to 10 inch (25 cm) as representative gap heights [12]. Thus, the gap heights to be tested are: 10 cm, 15 cm, 17 cm, 20 cm and 25 cm. The PMMA sample set-up and the laboratory jack is then mounted on a mass balance in order to record the mass loss during the test process. A video camera is installed to capture the experiment as the primary means for quantitative determination of the flame spread process by monitoring the flame front, burn-out front as well as the flame characteristics i.e. flame height, pyrolysis length. The final set-up is shown in Figure 9.

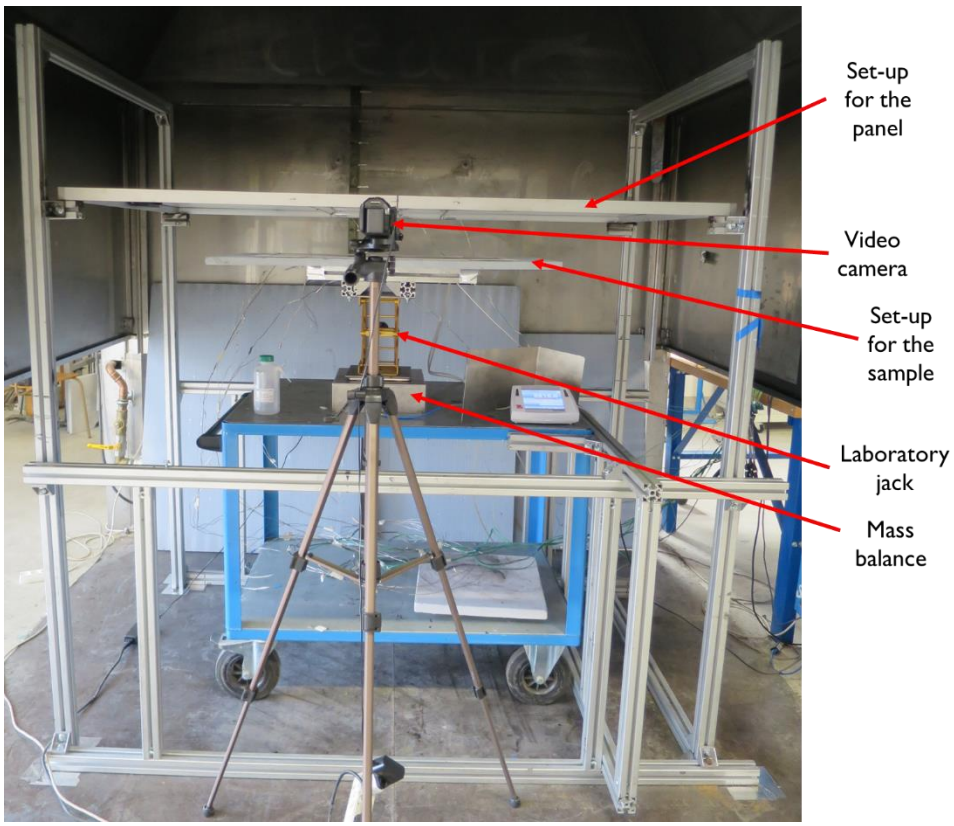


*Figure 9 Final Set-up*

## 2.3 EXPERIMENTAL PROCEDURE

Table 2 shows the experimental matrix for the tests that would be analysed in this study.

*Table 2 Experimental matrix*[6]

| ***Test No.*** | ***PV panel height (H)*** | ***Panel material (P)*** |
|---|---|---|
| *1* | No panel | No Panel |
| *2* | 25 cm | Stainless steel surrogate |
| *3* | 20 cm | Stainless steel surrogate |
| *4* | 17 cm | Stainless steel surrogate |
| *5* | 15 cm | Stainless steel surrogate |
| *6* | 10 cm | Stainless steel surrogate |
| *7* | 20 cm | PV Panel |
| *8* | 17 cm | PV Panel |
| *9* | 15 cm | PV Panel |

The mass balance was zeroed at the start of each test. Simultaneous ignition along the entire edge of the PMMA sample as achieved by igniting the strip of ceramic paper along the ignition end of the sample that has been evenly laced with 15 g of methanol shown in Figure 10. The onset of PMMA ignition was indicated when the mass readings reaches a zero value after the methanol had completed burning and flame spread process was observed on the adjacent PMMA. The measurement points from the thermocouples in the PMMA, thermocouples in the gap, heat flux gauge and mass balance were logged every 2 seconds from the start of ignition of the PMMA until the entire PMMA sample was burnt out.

[6] See Appendix 2 for full experimental matrix including preliminary tests carried out.

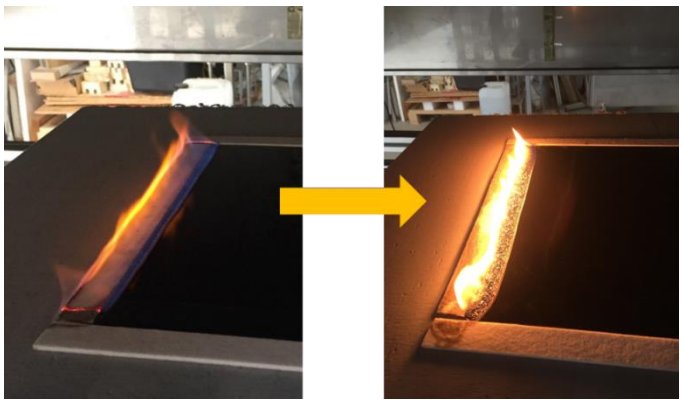

*Figure 10 Simultaneous linear ignition along ceramic paper (left) eventually ignite the PMMA (right)*

*Figure 11 Progress of the experiment was monitored*

## 2.4 VIDEO ANALYSIS METHOD

The flame spread rate was not directly measured and video analysis was carried out in order to quantify the trends observed visually. The centreline of the sample was used as a reference point for all tests when obtaining the data from the video footage. To facilitate the discussion, reference point, x, would refer to the distance from the ignition edge of the panel while reference point, $x_f$, would refer to the distance from the moving flame front.

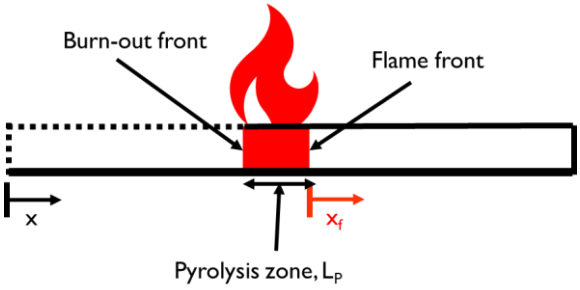


*Figure 12 Reference points for discussion*

The flame spread rate was derived through monitoring of the front of the pyrolysis zone in terms of the taken for the flame front to travel between two consecutive marks indicated on the video footage. The time stamp when the flame front and burn-out front reached every 5 cm interval was recorded from the video observations. The widely used indicator of the advancing pyrolysis zone for PMMA is the point where there is first appearance of sub-surface bubbling [16]. This method was used by Orloff et. al. to monitor the advancing flame front by visual observations of surface bubbling seen through a clear PMMA slab [30]. Although the PMMA slab used in our experiment is black and opaque, observations of bubbling on the surface would suffice especially since the PMMA sample is thin. The burn-out front is monitored when the trailing edge of the pyrolysis zone characterised by surface bubbling reaches the measurement point. Figure 13 shows a still frame to illustrate how the flame front position was monitored.


*Figure 13 Example of how record of flame front is monitored*

Video analysis was also used to quantify the flame heights, flame extension length under the panel (if any) and the pyrolysis zone. Still frames based on the time stamp used to determine flame spread rate every 5 cm was obtained and the flame length ($L_f$), pyrolysis length ($L_P$) and flame extension ($L_e$) were obtained from scaled measurements of these video footage. Figure 14 shows a still frame to illustrate how these measurements were obtained.

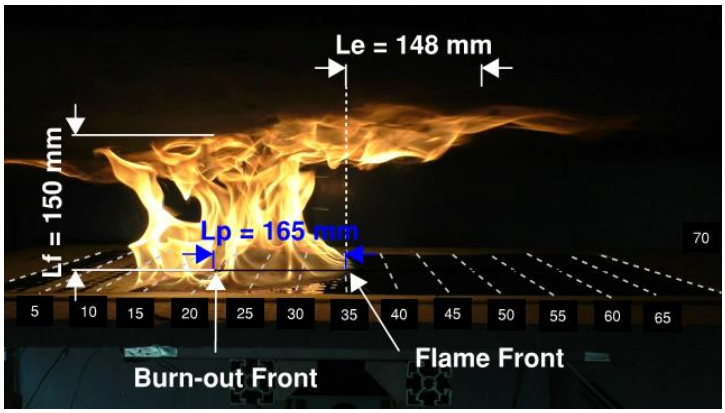


*Figure 14 Example of how the different measurements were obtained*

# 3 EXPERIMENTAL RESULTS AND DISCUSSION

Tests 1-6 with the PV surrogate are discussed first before comparisons with Tests 7-9 involving actual PV panels are analysed in Section 3.7.

## 3.1 VISUAL OBSERVATIONS

Visual observation during the experiments demonstrated that after a short initial transition period whereby the flames from the burning ceramic paper spread to the adjacent PMMA sample, the flames assumed a pronounced structure as shown in Figure 10. However, as the flame continue to propagate along the sample for the different tests with decreasing gap height, a significant change in fire spread behaviour was observed when the gap height reached a critical value.

In the free burning situation, the flame propagation continued with a constant but slow rate and did not show signs of extinction or growth until complete burn-out of the sample. The flame front maintained a fairly linear horizontal profile although there are slight curvatures along the edges due to the lateral airflow that shortens the rising flames near the sides of the sample. This reduces the radiative heat transfer from the flames to the sample and hence, reducing the flame propagation rate along the edges giving rise to the curved flame front observed. The flames have a laminar structure with a constant flame height and area of burning fuel (pyrolysis zone). A similar steady state was observed with the introduction of the PV surrogate panel at gap heights of 25 cm and 20 cm with the flames propagating at a constant rate after a short growth at the start albeit the flame spread rate was slightly faster. The curvatures of the flame front near the edges are more pronounced with the panel as the effect of panel is more enhanced along the centre of the sample. The flames have a more turbulent structure with wrinkled flames as the panels changes the flow of entrained air to the flames. Although the flames also achieve a constant height and pyrolysis zone area, a slight increase was observed compared to the free burning situation. However, the height of the flame is maintained below the gap distance. These effects caused by the panel are enhanced as the gap height decreases from 25 cm to 20 cm. Figure 15 shows the flame characteristics for these tests when the flame has spread to the mid-point of the sample (x = 35 mm). The time after ignition, t, at which the flames have propagated to this point also indicates the increase in flame spread rate with the introduction of the panel and at shorter gap heights.

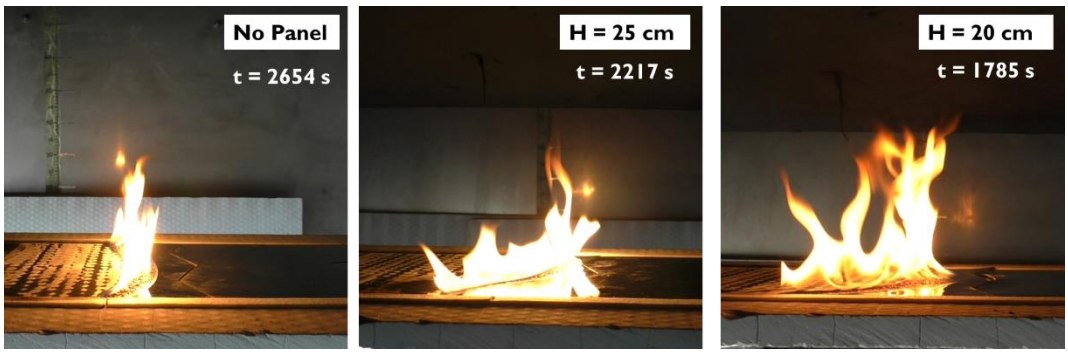


Figure 15 Observations of flames for Test 1-3 (see Table 2 shows the experimental matrix for the tests that would be analysed in this study.

*Table 2) when the flames reach mid-point of the sample (x = 35 cm).*

However, as the gap height decreases below 20 cm, these steady conditions could not be achieved. The progress of the fire for H = 17 cm, 15 cm and 10 cm can be classified into 3 stages as shown in Figure 16. In the growth stage, the fire showed a similar initial growth as the tests described above but did not reach a steady state as the fire continued to grow as observed though the steadily increasing flame height and pyrolysis zone area. The flame front seemed to be propagating at a comparable rate to the steady state cases discussed above. This slow growth continues until the flame impinge on the panel and the onset of flame deflection under the panel was observed. As the gap height decreases, the time taken for the flame to reach a point of deflection under the flames also decreases indicating that a shorter gap height would result in a faster transition to the accelerated stage. The flame spread accelerates rapidly upon flame impingement and the burning zone expands. The flame propagated along the sample at a much higher rate and the burning PMMA behind the flame front burnt vigorously as the sub-surface bubbling is enhanced compared to the growth stage as shown in Figure 17. As the size of the bubble generated is dependent on the heat flux on the fuel surface [31], it can be derived that the mass burning rate and intensity of burning is high in the accelerated stage. The length of flame extension deflected under the panel continues to increase radially even past the length of the panel.

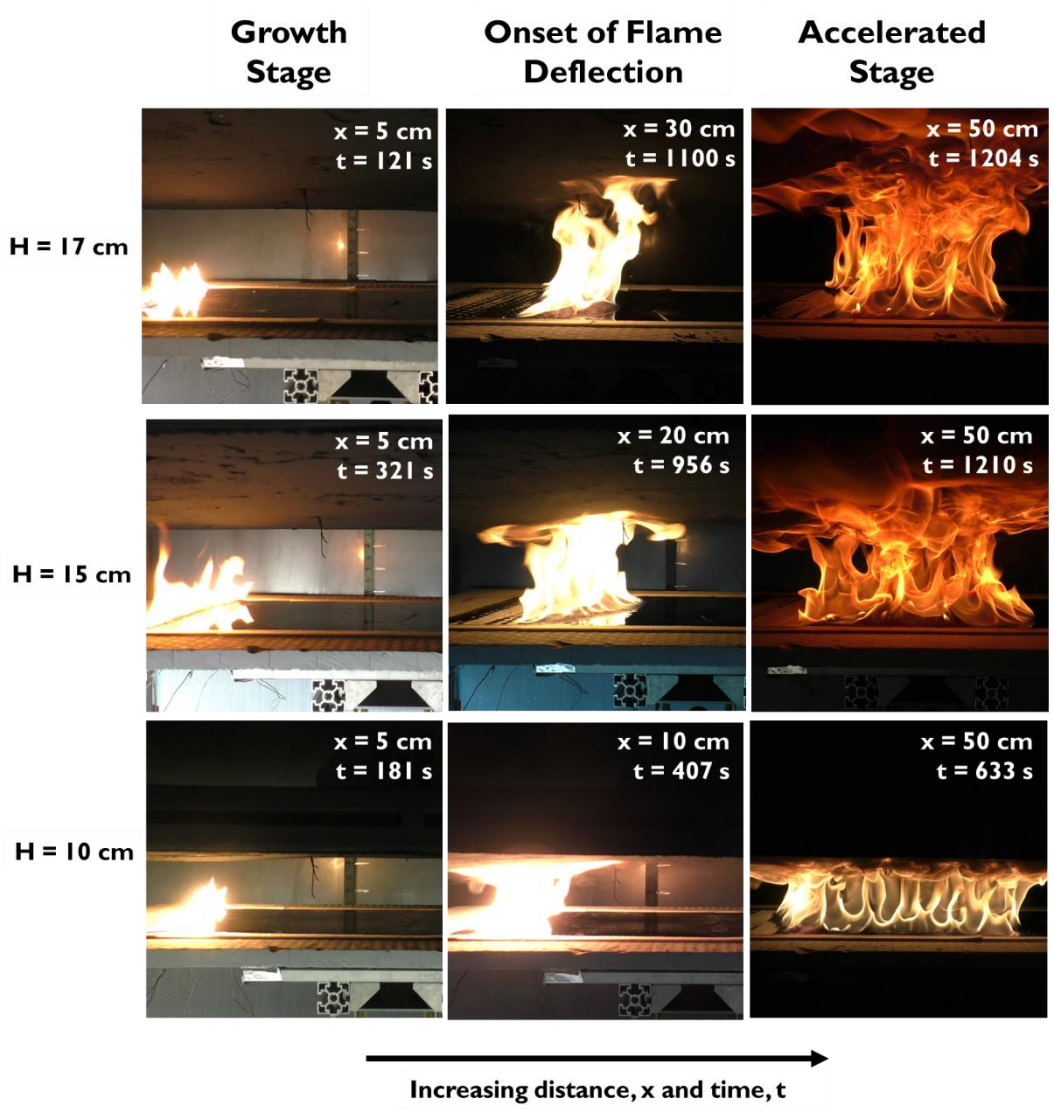


*Figure 16 Flame observations for Test 4-6 (H = 17 cm, H = 15 cm and H = 10 cm)*

*Figure 17 Surface bubbling in the growth phase (left) and the accelerated phase (right)*

Through these visual observations, there is a strong correlation between the flame spread and fire growth indicated by the observations on flame height and pyrolysis zone. Furthermore, a distinct difference was observed for test with no panels, H = 25 cm and H =

20 cm compared to tests with H = 17 cm, 15 cm and 10 cm. The former set of tests reached a steady state characterised by a slow flame spread rate but for the latter set of experiments, there is a transition from a growing stage to an accelerated stage with rapid flame spread upon the deflection of the flames. A conceptual diagram capturing the observed characteristic of the flame spread is shown in Figure 18. Based on visual observations, there is indication of a critical gap distance between 17 cm and 20 cm, whereby flame spread characteristics will change such that the extent of damage in the event of the fire would be differentiated drastically between the two regimes. In order to analyse the observations quantitatively, measured parameters from the experiments would be discussed subsequently.

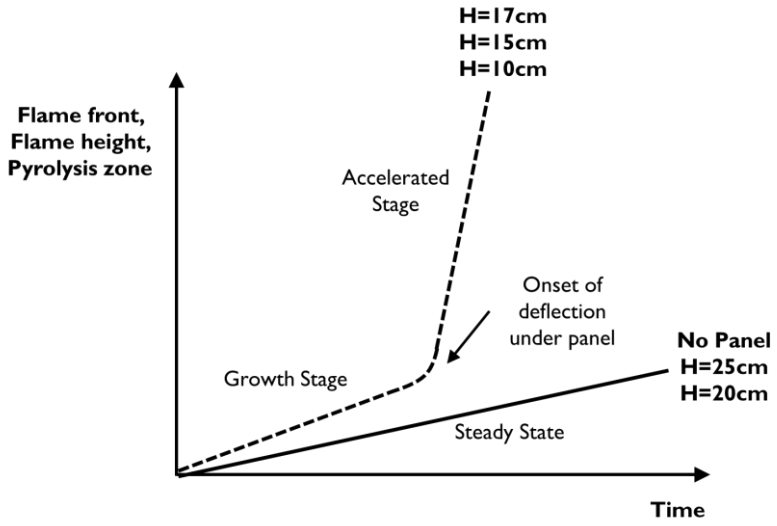


*Figure 18 Conceptual diagram of observations*

## 3.2 FLAME SPREAD RATE, FLAME HEIGHT AND PYROLYSIS ZONE

Based on video analysis, the propagation of the flame front over time was plotted as shown in Figure 19 whereby the gradient of the graphs would provide an indication on the rate of flame propagation along the surface. The results corroborate with visual observations whereby a constant flame spread rate is achieved for test with no panel and with installed panels at H = 25 cm and 20 cm as seen from the constant gradient of the best-fit linear graphs for these tests. The flame spread rates for these configurations is recorded in Table 3. The constant flame spread rate agrees with opposed flow horizontal flame spread theories explained in Section 1.2 as well as other experiments on opposed flow horizontal flame spread over PMMA sheets without the presence of the panel [28]. Although the flame spread rate increased with the introduction of the panel with a gap distance of 25 cm and a further increase was seen when the gap distance is reduced to 20 cm, the magnitude of the flame spread rate is relatively small and comparable for the free burning scenario without panel.

Thus, for H > 20 cm, the effect of the panel on flame spread rates is minimal. The constant and slow flame spread rates at these heights are not expected lead to extensive damage if detected early.

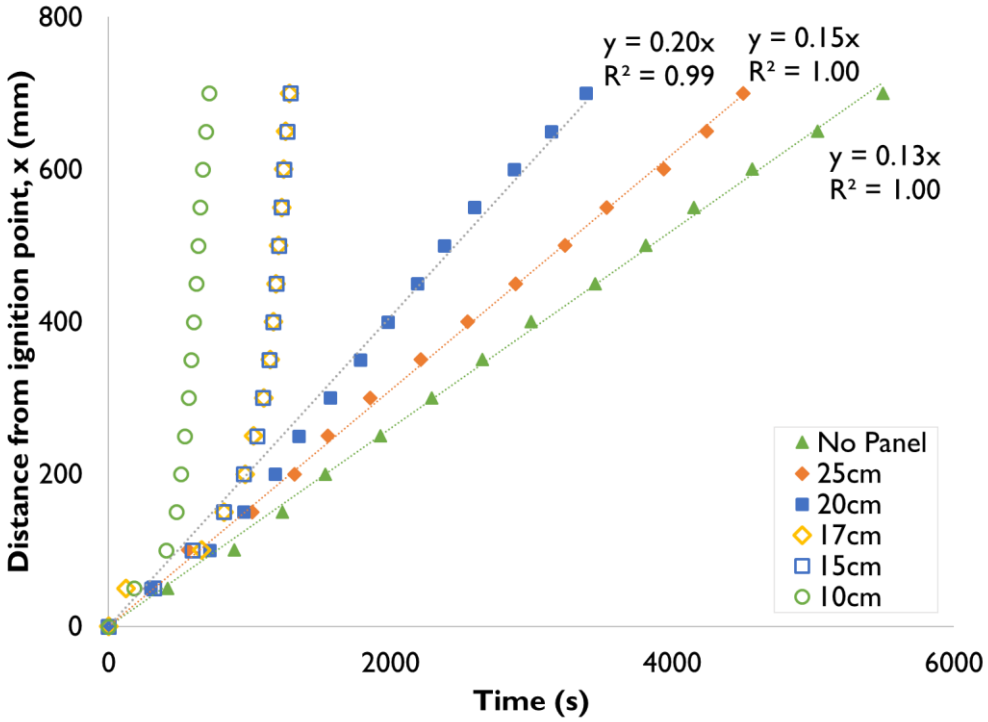


*Figure 19 Progress of the flame front over time for various panel heights*

However, for H < 20 cm, flames spread rates are not constant but instead accelerates rapidly as illustrated from the steep gradients reached for these tests. Figure 20 shows a focussed view on the results for tests of H = 10 cm, 15 cm and 17 cm. The flame spread rate seems to be relatively slow and constant at the start for all three experiments with rates comparable to the earlier steady state case of 0.18 mm/s to 0.25 mm/s. This growth stage continues until the point where the flames impinge on the panel and deflect under the panel causing an acceleration in flame spread. From the plot, the flame spread rate seems to accelerate until it reaches a higher constant rate of 2.7 mm/s for all 3 tests. The change in the dynamics upon the deflection of flames on the ceiling marks the transition from an opposed flow horizontal flame spread to a concurrent flow horizontal flame spread scenario since the flames extending horizontally beneath the panel result in an increased rate of heat transfer back to the sample which is more pronounced since flames have a higher temperature and emissivity compared to a hot gas layer and heated panel. Although the flame impingement preceding the accelerated stage would occur earlier for a shorter gap distance, the resultant effect for experiments with H = 17 cm, 15 cm and 10 cm is similar as they tend towards the same flame

spread rate. Thus, for H < 17 cm, the effect of the panel on flame spread rates is evident as the flame spread characteristics transit from a slow growing stage to a rapid accelerated stage upon flame impingement on the panel. The resultant flame spread rate that is more than 10 times the flame spread rate in a free burning situation highlight the influence of panels at these heights on the fire risk posed by PV installations. Below the critical gap distance, fires may be benign at the start of ignition but the rapid transition to an accelerated flame spread rate would result in an uncontrolled fire that could incur extensive damage.

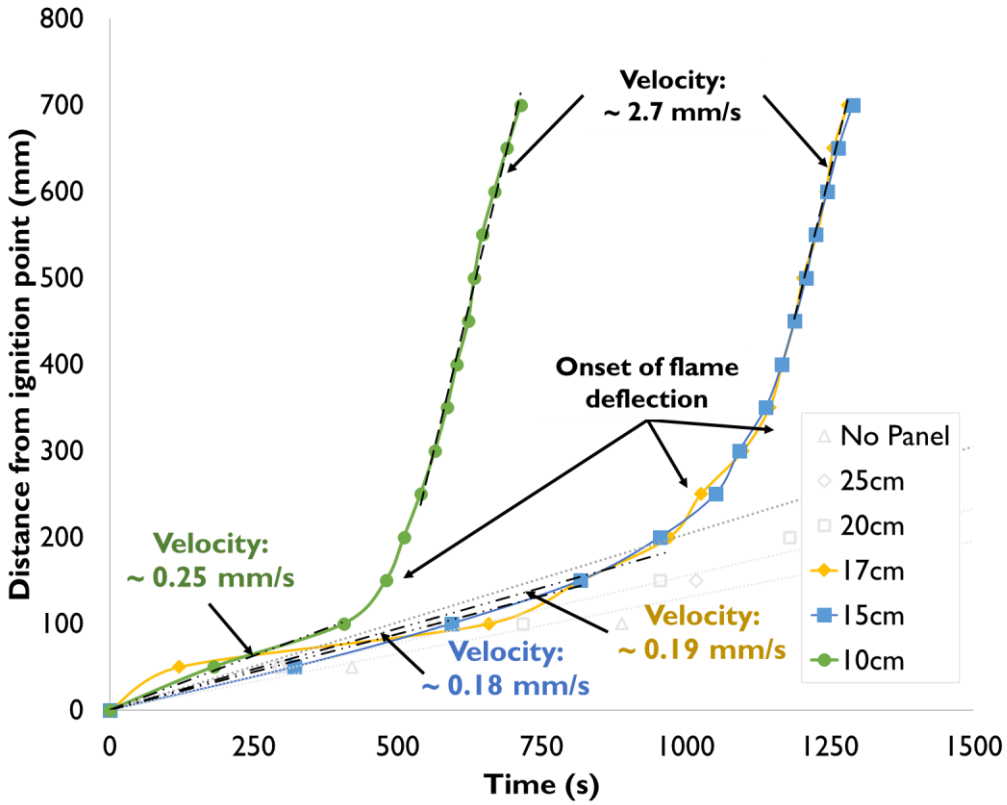


*Figure 20 Accelerated flame spread at the onset of deflection of flames under the plate*

These findings on flame spread rate highlights the limitation on current proposed test procedures for PV panels on roofs that are based on a criterion of maximum distance of flame spread in a pre-determined time interval. The existing classification test procedure (ANSI/UL 1703-2013) developed by Underwriters Laboratories (UL) takes into account the spread of flame between the PV panel, its racking system and the representative roof system in which an installed system passes the test if the flame spread is less than 1.8 m in 10 minutes [32]. From this study, the criteria dependent on a specific time interval would not be able to capture the hazard sufficiently especially if the time interval for testing is within the growing stage. In the current set-up, the flame would have only propagated for about 0.1 mm within 10 minutes for H = 17 cm, 15 cm and 10 cm as the fire is only in the growing stage. Thus,

under the current test procedure, the installations below the critical gap would have passed the test. However, the test failed to capture the occurrence of the subsequent accelerated flame spread rate thereafter which is critical in minimising damage. This highlights the need for the standard test criteria for PV installations on roofs to be reviewed in order to account for the observations in this study. PV installation classification tests should consider the impact of gap distances and its resultant flame spread behaviour when establishing the acceptable criteria.

In order to obtain a better understanding on the factors that are contributing to the difference in flame spread behaviours about the critical gap distance, other measured parameters were analysed.

Flame height would be analysed since an indicator of the transition to the accelerated stage is the point where the flame height exceeds the gap height. The relationship between heat release rate and flame heights can be derived from generic Heskestad's equations [33] by assuming the pyrolysis zone of the PMMA can be characterised as a pool fire. The pyrolysis zone which represents the burning area would also be quantified as it would reveal the growth of the fire. This can be represented as the pyrolysis length, $L_p$, given the constant width of the sample and relates to the heat release rate as shown in Equation (3). The burn-out front would also be used to analyse changes in the pyrolysis zone with time since the difference between the location of the flame front and the burn-out front at any instant in time would indicate the pyrolysis zone. The flame heights and pyrolysis lengths provide an indication on changes in the size or heat release rate of the fire especially since the heat release rate data was not specifically collected.

Flame extension length, $L_e$, under the panel will also be studied to analyse its role in the heat transfer process and predict the behaviour in the accelerated stage if applicable.

Flame heights and pyrolysis lengths obtained from tests without a panel, at H = 25 cm and at H = 20 cm did not show a noticeable trend over time. There is a wide distribution about the mean value due to the measurement technique adopted. However, visual inspection across the burning period shows that the flame heights and pyrolysis length are generally constant for each test and the mean value could be used as an indication of the average flame height pyrolysis length. Burn-out front was also plotted with the flame front as shown in Figure 21 to verify the findings of constant pyrolysis zone. As the burn-out front is moving with a similar constant speed as the flame front, a linear representation of the burn-out front can also be obtained for each test and the distance between the plots of flame front and burn-out front at any point of time would indicate the pyrolysis length.

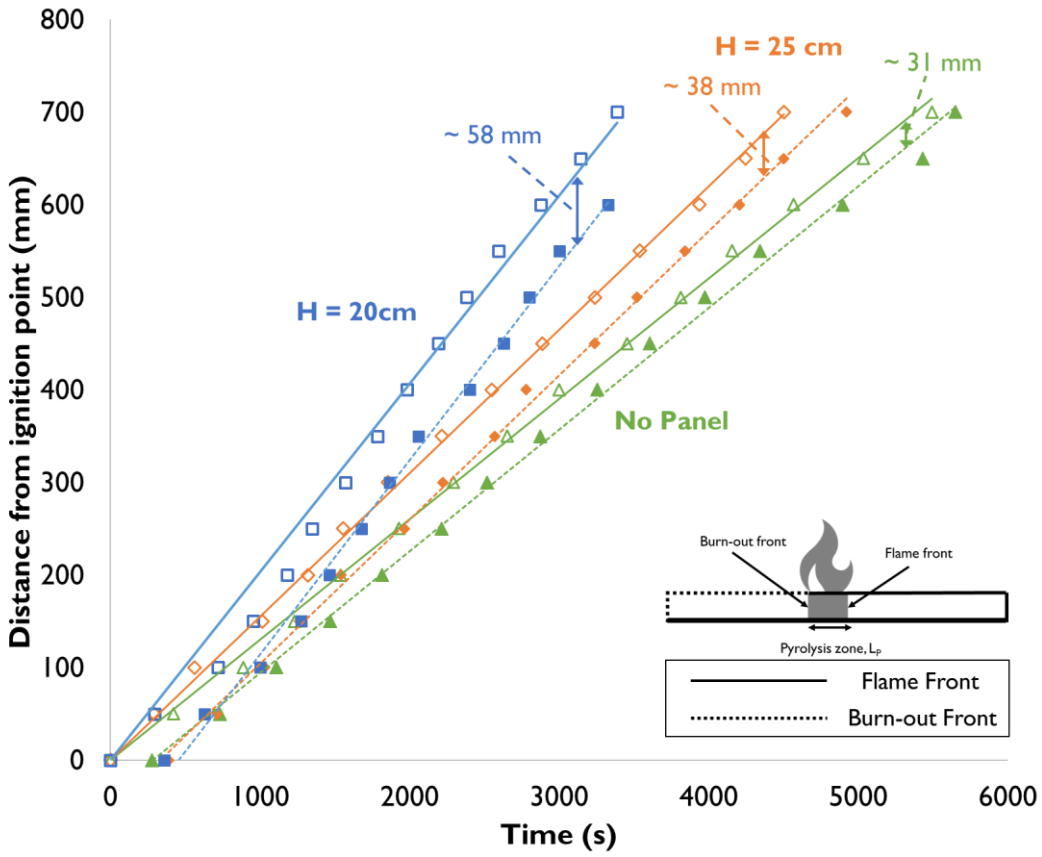


*Figure 21 Length of Pyrolysis Zone for Test 1-3 (no panel; H = 25 cm; H = 20 cm)*

A constant flame length and pyrolysis zone obtained in these experiments quantified in Table 3 indicates that a constant heat release was achieved i.e. it is not a growing fire. The presence of the panel at H = 25 cm and further lowering the gap distance to H = 20 cm results in a larger fire size although there is a balance reached in the system to achieve the steady state conditions. This further confirm the findings that when H > 20 mm, the flame spread rate would not constitute a major hazard not only due to the minimal increase in flame spread rate but also because there is a constant fire size.

*Table 3 Flame spread rates of test 1-3*

| Test No. | H (cm) | Flame Spread Rate (mm/s) | Flame Height, $L_f$ (mm) | Pyrolysis Length, $L_P$ (mm) |
|---|---|---|---|---|
| **1** | No Panel | 0.13 | 72 | 31 |
| **2** | 25 | 0.15 | 92 | 38 |
| **3** | 20 | 0.20 | 109 | 58 |

However, this behaviour did not hold when the gap distance decreases to 17 cm, 15 cm and 10 cm. The flame height, flame and burn-out front are plotted with the flame extension, $L_e$ and pyrolysis length, $L_p$ indicated. Pre-heating time, $t_f$ and the burnout time, $t_b$ was also

indicated in the plots. Pre-heating time refers the time at which any point on the sample is exposed to pre-heating from the extended flame before ignition and burn-out time refers to the time for any point of the sample to complete burning after ignition. These are illustrated in Figure 22, Figure 23 and Figure 24 for H = 17 cm, 15 cm and 10 cm respectively.

The plots show the accelerating nature of the flame spread process. In the growth stage for all three tests, the pyrolysis length and the flame height gradually increase with time which indicates a growing fire until the point where the flame height impinges on panel and deflect causing the accelerating nature of the spread. It was found that within the accelerated stage after flame deflection, the pre-heating time of the flames ($t_f$) and the burn-out time ($t_b$) form the characteristic time of this phase since it remained essentially constant. The curves of the flame extension end, flame front and burnout front against time have identical shapes and are related to each other by shifts of $t_f$ and $t_b$ respectively along the time coordinate. From the plots, the resultant flame spread rate in the accelerated stage tends towards an asymptotic value of a constant spread rate as which has also been suggested in Figure 20. These findings concur with characteristics of concurrent upward flame spread. Experiments on upward flame spread on thin materials such as paper and textiles showed similar trends ([34], [35]) whereby the spread of flame initially accelerates due to the increases in the pyrolysis and flame lengths but as the burn-out rate increases due to the enhancement of the burning rate, the flame spread rate becomes constant as the burn-out front and flame front velocities approach each other. These finding indicate that below the critical gap distance, there is negligible effect in further reducing the gap distance as the flame spread rate remains at the same constant rate. The constant burn-out time also indicate that the resultant heat release rate of the fire is independent of the gap distance below the critical gap distance. Since there is negligible difference in the resultant effect on flame spread rate and fire growth when reducing the gap distance below the critical gap distance, it is essential to define the critical gap value as it would be considered the worst-case scenario.

The difference in flame and burning characteristics between the two sets of tests highlight the importance of identifying the critical height above which accidental fires would not cause a rapid flame spread. The resultant flame spread rate reached from test with H < 17 cm is almost 2 orders of magnitudes faster compared to the constant flame spread rate reached when H = 20 cm. Compared to the free burning scenario, there is no drastic changes in the flame spread characteristics when the panel is placed at H = 25 cm or H = 20 cm. Similarly, the decrease in gap height from 17 cm to 10 cm did not seem to affect the resultant flame spread rate reached although the growth stage is more rapid at shorter gap heights. Thus,

establishing the critical height at which the flame spread would not transit from a typical opposed flow horizontal flame spread to a concurrent flow which is more rapid is important in fire safety considerations of PV installations on roofs.

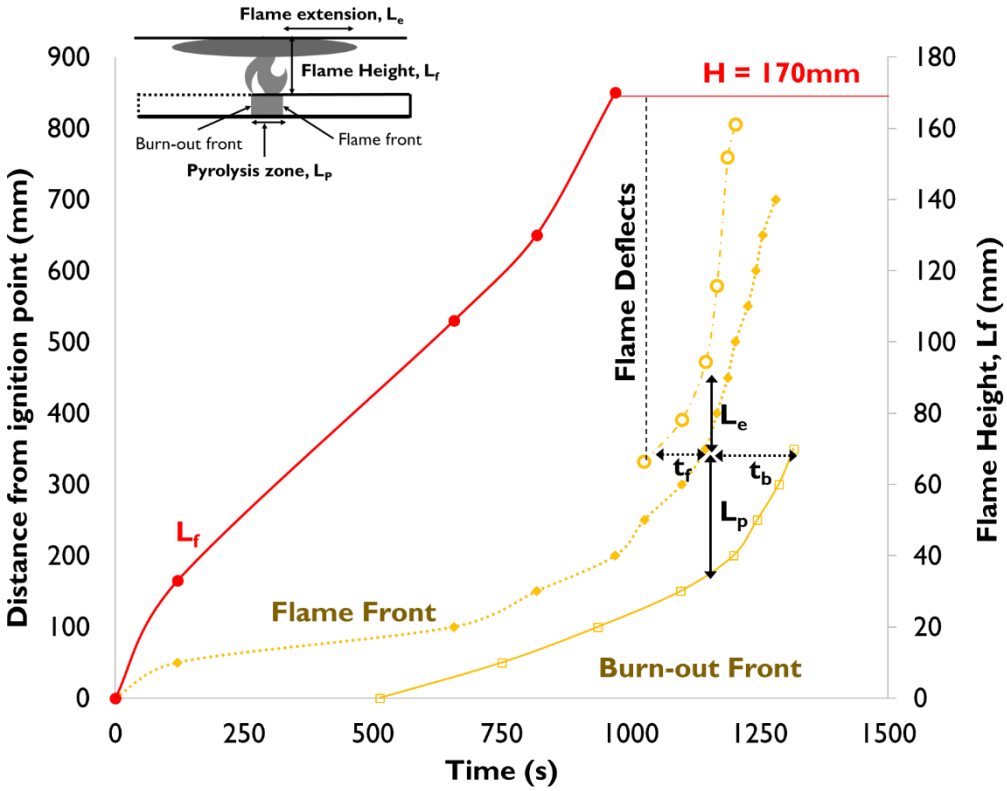


*Figure 22 Flame characteristics over time for Test 4 (H = 17 cm)*

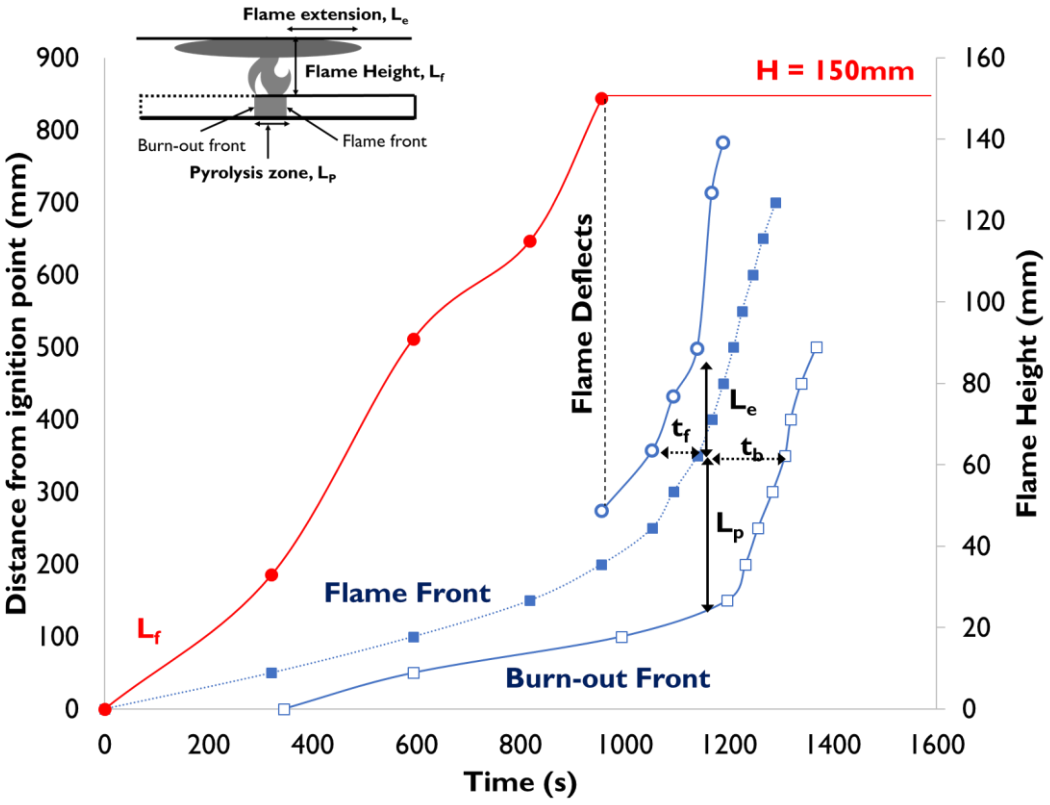


*Figure 23 Flame Characteristics over time for Test 5 (H = 15 cm)*

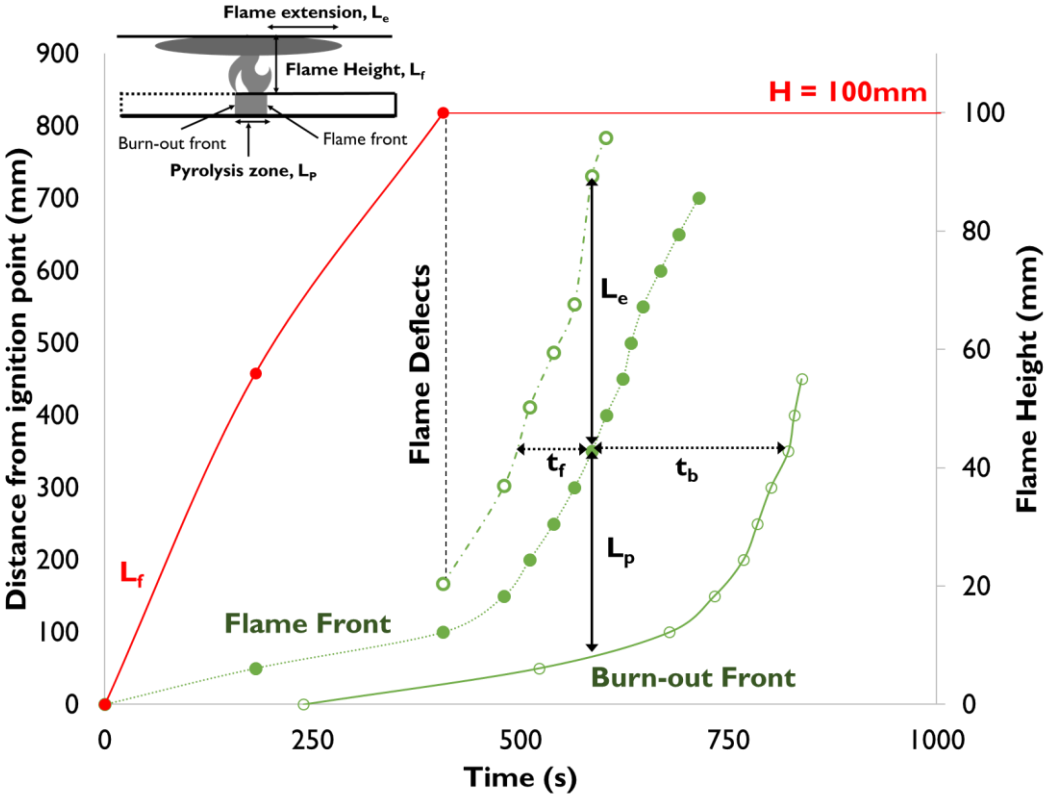


*Figure 24 Flame Characteristics over time for Test 5 (H = 10 cm)*

### 3.2.1 Validation of results and limitations

While the video observations provided the source for all quantitative data on flame spread, the thermocouple records obtained in the experiments confirmed with the data in the video analysis. Figure 25 shows the thermocouple traces for Ts2 and Ts 6 in Test 5 as a representation of the concurrence between video and temperature readings in determining flame front and burnout front. The flame front is seen to correspond to the sudden rise in temperature at about 100°C. This temperature is lower than melting point of PMMA (~160°C [16]) and is ahead of the reduction in rate of temperature rise that typically indicate pyrolysis onset. This can be attributed to the thermocouple lag time since larger gauge size was used to facilitate the experimental set-up. The burn-out onset was more clearly correlated to the sudden temperature drop after the maximum temperature was reached. Thus, the temperature history, depicted by the thermocouple records generally agreed with visual observations. As the temperature probes are only located within the central area of the sample, the use of temperature history to chart the flame spread would not be able to capture the growth stage of the fire which is important in the study of flame spread and fire growth in smaller gap distances as seen in experiments with H < 17 cm. Thus, visual observations remain the primary means of determining the progress of the flame and burn-out front.

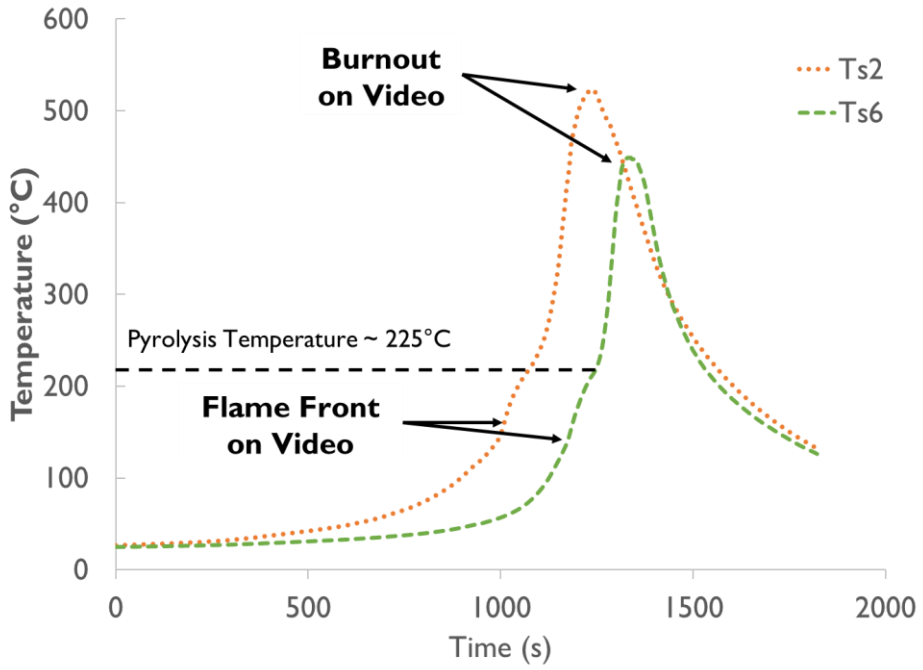


*Figure 25 Thermocouple records for flame spread (Test 5: H = 15 cm)*

However, the method in the analysis by only capturing still frames from specific intervals (every 5 cm) of the tests may not provide a true representation of characteristics of the flame

for the whole interval although the trends fit with data verification with temperature data. This is especially disadvantageous in the analysis of the rapid growth stage as minimal data points are available to form an understanding on the processes driving it. An attempt was made to analyse the video recording with a MATLAB binary image processing code in order obtain a better spread of data. However, due to the reflection of the flame onto the PMMA sample at the start of the burning, the image processing code was unable to capture the flame front accurately for the growing stage. Similarly, due to the light exposure of the surroundings, meaningful results could not be obtained for flame heights, extension and pyrolysis zone through this method. However, there is a close agreement between the image processing and video observations which supports the use of visual observation to study general trends of the flame spread and its characteristics.

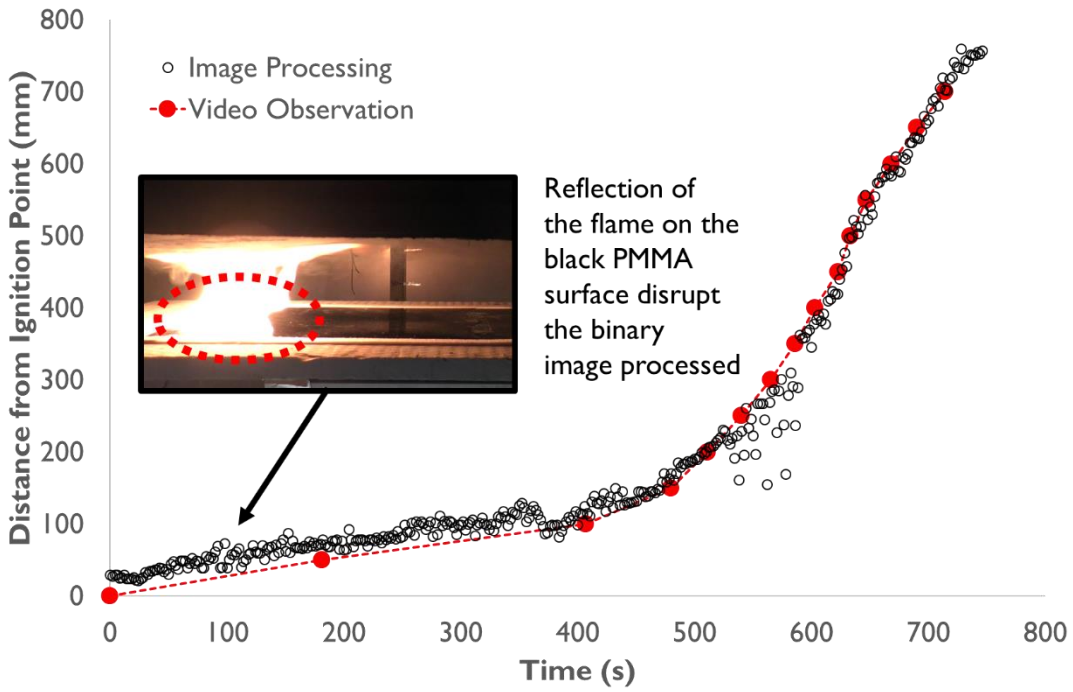


*Figure 26 Comparison of image processing and visual observation data for Test 6 (H = 10 cm)*

An accurate knowledge of the relative position of the flame front with respect to the location of the measurements is critical in the interpretation of the results. Future studies could employ more sophisticated methods of determining the flame front. Ray et al. used an optical indicator which capitalise on the properties of clear PMMA whereby the virgin PMMA material would be transparent to light while the burning region is opaque [19]. A more accurate determination of the position of the pyrolysis front was also developed by Pizzo et al. using a processing method based on wavelet decomposition from video recordings of the

bubbling surface that could improve the reproducibility and provide a more systematic experimental procedure [31]. This could potentially improve measurement of the pyrolysis zone length. However, this is deemed not required for the current preliminary studies but would be critical in future detailed analysis of the system.

## 3.3 Mass Loss Rate Measurements

Based on the visual observations and analysis of flame characteristics, indications in terms of changes in pyrolysis length and flame height suggest that the heat release rate changes due to the introduction of the panel compared to a free burning scenario and varies with gap distance. Thus, an analysis of the mass loss rate of the sample would be able to support these observations. Figure 27 shows the how the mass of the sample changes with respect to time as the flame propagates along the sample.

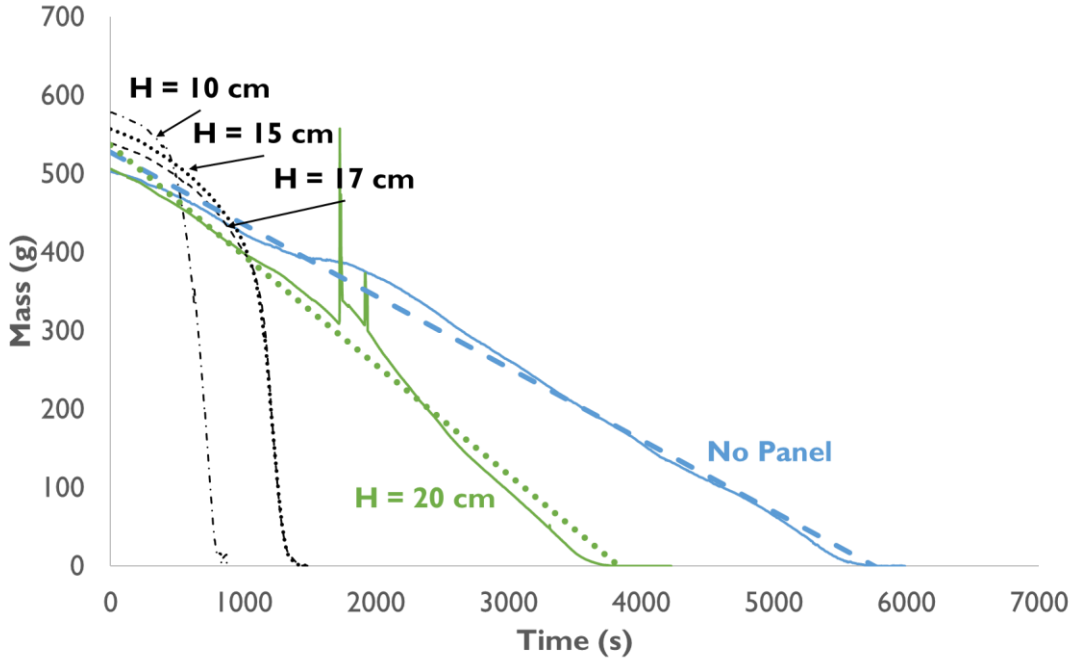


*Figure 27 Mass readings versus time*

A relatively constant mass loss rate was observed for tests with no panel and test with H = 20 cm as shown from its relation to the best fit linear graph[7]. Mass loss rate was deduced through the gradient of the best fit linear graph and validated with calculations stipulated in ISO 5660 which includes the "main" burning period i.e. from 10% of ultimate mass lost to 90% [36]. Based on comparisons between these two tests, the mass loss rate increases with the presence of the PV panel. As it was not possible to obtain heat release rate (HRR) from

[7] Mass readings for test 2 with H = 25 cm was not recorded.

the oxygen calorimetry, mass loss rate could also be used to provide an indication of the heat release rate considering the assumption of complete combustion that does not account for combustion efficiency. Thus, it could be deduced that with a constant flame spread, a constant HRR is generally obtained. This agrees with the deduction from the analysis of flame heights and pyrolysis zone. The presence of the PV panel not only increases the rate of flame spread but also increases the heat release rate even though the burning characteristic of the material is the same. However, compared to the tests of H < 20 cm, the difference between these two tests is not considered to be critical.

*Table 4 Mass Loss Rate for Test 1&3 (No Panel; H = 20 cm)*

| Test | H (cm) | Mass Loss Rate from graph (g/s) | Mass Loss Rate Calculated (g/s) |
|---|---|---|---|
| **1** | No Panel | 0.09 | 0.09 |
| **2** | 20 | 0.14 | 0.15 |

On the other hand, the mass loss rate for tests H < 20 cm is not constant but follows the same trend as that seen in the flame spread rate. The mass loss rate for these tests are shown in Figure 28. Mass loss rate was calculated using the five-point numerical differential equations for each time step [36]. In order not to capture the decay stage of the burning, the mass loss rate calculation was carried out until the point when the flame front reaches the end of the sample. A 20-point average trendline was plotted. The mass loss rate increases in a gradual rate during the growth stage till a certain point which corresponds to the onset of deflection of flames on the panel. Thereafter, the mass loss rate increases rapidly linearly. From the plots, the mass loss rate starts to fall after reaching a maximum mass loss rate of about 2 g/s although it cannot be determined whether this is due to the onset of burn-out of the fuel since the flame has propagated towards the end of the sample or that mass loss rate would reach a maximum value.

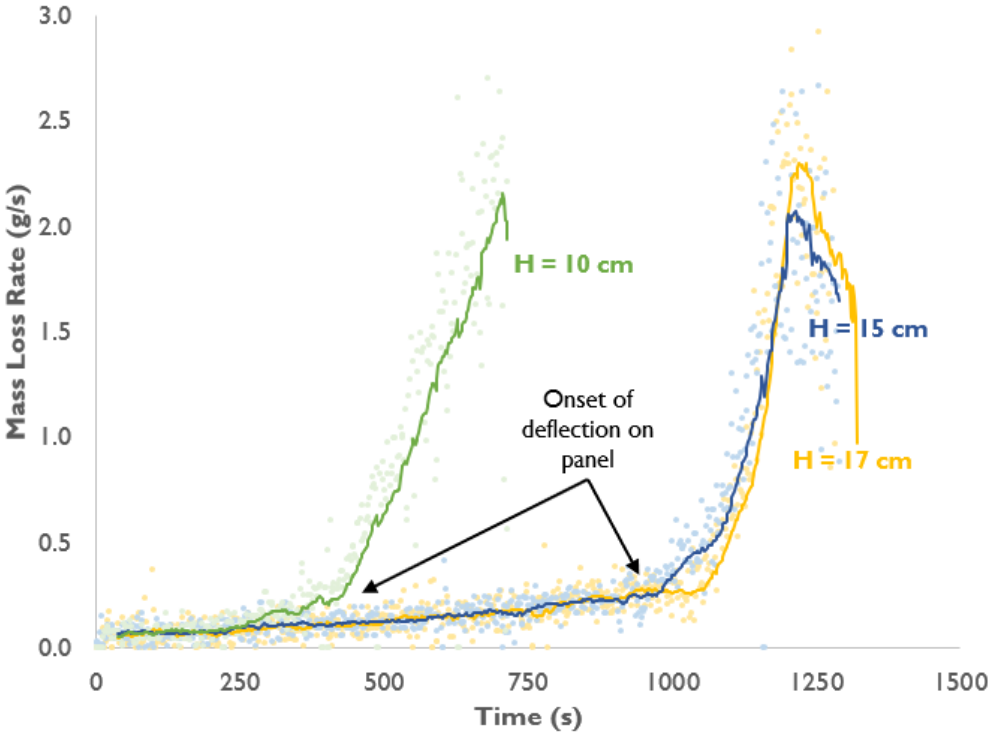


*Figure 28 Mass Loss Rate for Test 4-6 (H = 17 cm; H = 15 cm; H = 10 cm)*

From the mass loss data, we can deduce similar conclusions to the flame spread rate data. The critical gap distance which cause a massive change in flame spread behaviour would also affect the fire growth. In order to quantify the impact, equation (3) is used to obtain the maximum heat release rate from our set-up assuming complete combustion given that $\Delta H_c$ of PMMA is 24.89kJ/g [16]. The free burning scenario produced a fire with a constant HRR of 2.2 kW which increased to 3.7 kW with a panel at H = 20 cm. This increase is negligible especially since it is coupled with a low flame spread rate and the fire did not show signs of growth. However, the set-up had the potential to grow to almost 50 kW when the gap height is lowered to 17 cm, 15 cm and 10 cm. Although the absolute value of HRR should not be concluded based due the assumptions made, the increase in of the fire size from the order of 2kW to 50kW when the gap height is reduced below the critical height should be acknowledged. The results seem to show that further lowering of the gap distance below 17cm did not seem to aggravate the fire further as the increase in mass loss rate and the maximum mass loss rate reached after deflection of the flames seemed to be similar for tests with H = 17 cm, 15 cm and H = 10 cm. Thus, identifying the critical gap distance is not only important in limiting the flame spread rate but also limiting the eventual fire size as a significantly larger fire size would lead to more intense conditions in terms of temperatures and heat flux. These conditions would make it more difficult to control the fire especially

coupled with a rapid flame spread rate. Thus, installations should not fall below the critical gap distance such an undetected small fire within the gap would not be allowed to spread and grow substantially such that it becomes difficult to control.

### 3.3.1 Verification of results and limitations

A simple calculation was done to validate the results between the mass loss and the flame spread rate. Through the conservation of mass, given a constant flame spread rate and mass loss rate, the mass loss of the fuel, $\dot{m}_{loss}$, should equal the mass of the newly pyrolyzed fuel, $\dot{m}_{pyrolysed}$ ahead of the flame for every instant in time. The calculations are shown below and the results are tabulated in Table 5.

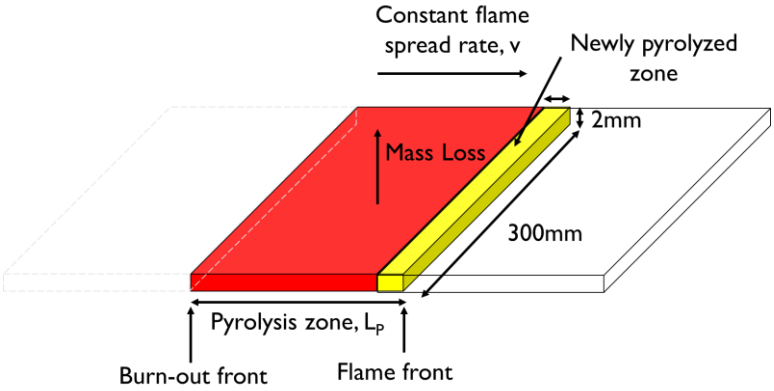


*Table 5 Verification of mass loss rate data*

| Test No. | $\dot{m}_{loss}$ (g/s) | $v$ (mm/s) | $\dot{m}_{pyrolysed}$ (g/s) |
|---|---|---|---|
| **1 (No Panel)** | 0.09 | 0.13 | 0.09 |
| **3 (H = 20 cm)** | 0.15 | 0.20 | 0.14 |
| **4 – 6 (H = 17 cm, 15 cm, 10 cm)**[8] | 2 | 2.7 | 1.92 |

Thus, the mass loss rate data corroborate with the flame spread rate data obtained for constant burning situations.

Although the trends from the mass loss rate data can be verified with the flame spread rate data, the mass readings itself may be erroneous. There are instantaneous disturbances during

[8] These are for the resultant flame spread rate and the maximum mass loss rate obtained in the accelerated stage for these test.

the test with H = 20 cm which caused discontinuous measurements as shown in Figure 27. Furthermore, it was also found that the mass balance had a drifting measurement that did not observe a certain trend. The initial mass of the sample also varied for each experiment within the range of 514 g $\pm$ 2%. Thus, the mass loss readings will only be used to analyse the trends between each test and will be not analysed in absolute terms.

## 3.4 SURFACE TEMPERATURES MEASUREMENTS

From the findings on flame spread rate and mass loss rate, we can establish that there is a critical gap height for PV installations on roofs below which the is a risk of rapid flame spread and fire growth should a small fire occur within the gap. To understand how this change in fire spread behaviour could transition to an accelerated stage, temperature measurement points in the sample is analysed. As discussed in Section 1.3, the effect of the introduction of a panel above a burning surface is the resultant imposed radiative heat flux which seeks to pre-heat the surface before the arrival of the flame front thus increasing the rate of flame spread. Fernandez-Pello and Hirano claimed that the constant flame spread rate will only occur if the external radiation balances the heat losses from the surface i.e. if the surface temperature ahead of the flame at any instant is kept constant [37]. Thus, the pre-heating phenomenon will be analysed through surface temperature measurements.

The temperature profile within the sample as the flame progresses was plotted based on the average temperature over the time taken for the flame to travel 5 cm. Figure 29 shows the temperature profile within the PMMA as the flame progresses along the sample. Raw data of the temperatures are shown in Appendix 3.

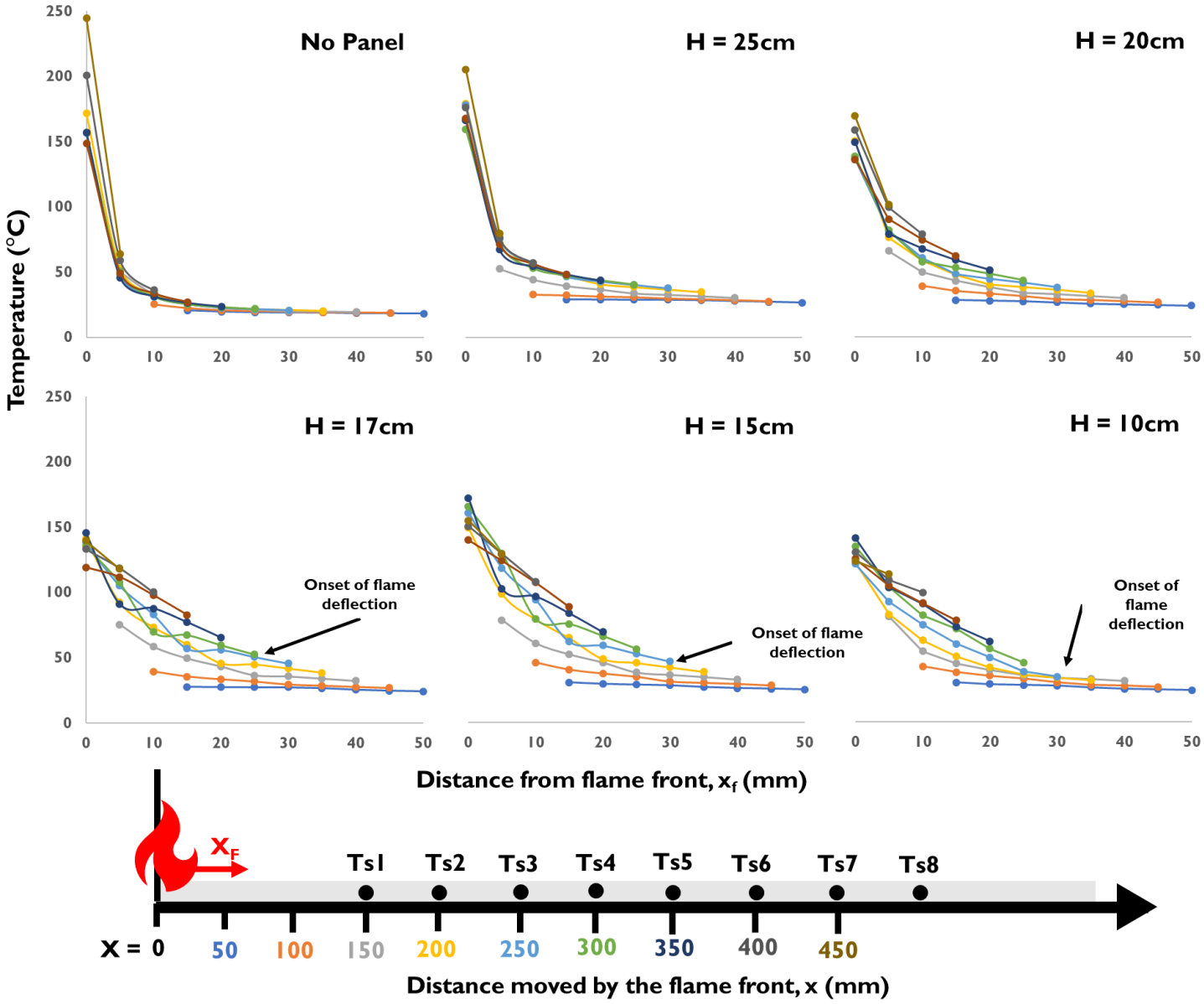


*Figure 29 Temperature profiles of the PMMA sample*

Without the panel, there is a constant pre-heating length of 20 cm as the flame propagates beyond which the temperature remains at ambient. This supports the results earlier that there is a constant flame spread rate achieved since the pre-heating length is constant and the temperature profile within the sample is maintained at every time step. With the introduction of the panel at H = 25 cm, a similar profile was achieved with a longer pre-heating length after the flame has propagated 10 cm. There is a slight growth phase within the first 15 cm of the flame spread but it eventually reached a constant surface temperature from the flame front as shown by the converged temperature profiles. As the gap height decreases to 20 cm, the temperatures increase as the flame propagates along the sample although a similar profile was maintained. This suggests that the temperatures within the PMMA downstream from the flame front is progressively increasing though it seems to reach a stable profile after the flame has propagated 30 mm. However, there is not insufficient data points further along the PMMA sample to verify this. Generally, these tests showed a similar temperature profile with a steep gradient near the flame front that tapers off further away. Even with the presence of the panel at these heights, the effect of temperature increase is focussed in the area near the flame which is related to the ceiling jet temperature distribution. As the surface temperature increases, radiative heat loss increases such that it would balance the imposed heat flux acting on the surface and constant flame propagation rates is achieved.

However, when the gap distance decreases to 17 cm, 15 cm and 10 cm, there is change in the surface temperature profiles. At the start of the propagation, the profiles are similar for all tests. Upon the onset of flame deflection, the temperature gradient near the flame front reduces and the surface not only preheats to a higher temperature but also across a larger span. For example, the surface temperature at 10 cm away from the flame reaches 100 °C for tests with gap distances of 17 cm, 15 cm and 10 cm while for the earlier 3 tests, temperatures are kept below 50°C. With such pre-heated surface temperature, less heat is required to increase the temperature to ignition point resulting in high flame propagation rates. The gentler temperature gradient also suggests that the high preheating temperatures would be extended further along the sample although there are not enough data points along the sample to quantify the pre-heated length. There also seem to be a convergence towards the end of the measured data which may support the findings earlier that a constant albeit fast flame spread rate was achieved. This convergence which occur after flame deflection could be attributed to the pre-heating due to the direct radiation from the horizontal flame deflection above the sample. As temperature of the horizontal flame is high and the gap distance is sufficiently low, the resultant radiative heat flux from the flames to the sample will not vary significantly with decreasing gap distance. Thus, since the pre-heating from the

deflected flames is independent of the gap distance, resultant flame spread rates would also be independent of the gap distance below the critical gap distance.

The temperature profiles obtained from the temperature profiles corroborate with the findings from observations of flame spread as well as mass loss rate. The constant spread rates obtained for the first 3 tests agree with the constant surface temperatures downstream of the flame front though. Similarly, this was observed for the accelerated stage. However, as the thermocouples are placed 15 cm away from the ignition point and the growth stage occurred mainly within 15 cm from ignition, there is insufficient points to investigate the temperature changes in the slab in the growth stage to determine the effects of surface temperature that would result in the growth of the fire before onset of deflection.

### 3.4.1 **Limitations of Results**

Although the thermocouples readings were able to provide an obvious trend, discrepancies in the thermocouple readings raise the question of the accuracy of the absolute readings. The growth phase that was captured in H = 25 and H = 20 cm but not evident in the flame spread and mass loss readings seem to suggest that the thermocouple lags the actual rise in temperature of the PMMA. This is also evident through the maximum temperatures recorded at the flame front. The maximum temperatures were higher when the flame spread is slower (i.e. test with no panel) and decreases as the flame spread increases. These could be attributed to the thermocouple lag since a larger thermocouple tip was used.

Furthermore, the installation of the thermocouple within the PMMA to capture its bulk temperature is not consistent with every thermocouple. This could be seen in the dip in thermocouple reading for H = 17 cm and H = 15 cm for Ts5 which is due to the thermocouple being closer to the insulation and may not be capturing the temperature of the PMMA. It is also observed that at high temperatures the PMMA sample warps due to uneven heating which may cause it to lose contact with the thermocouple. For test with H = 10 cm, the gap between the PMMA sample and the insulation during warping caused flaming on the underside of the sample. Figure 30 shows how these transient flames characterised my periodical long tongues of flames along the underside of sample are formed when the sample warps. Bonding between the PMMA sample and the insulation board is critical to avoid this. These observations prove to be limitations in the use of the experimental set-up to obtain the actual temperature of the PMMA. However, trends could still be observed barring these measurement errors.

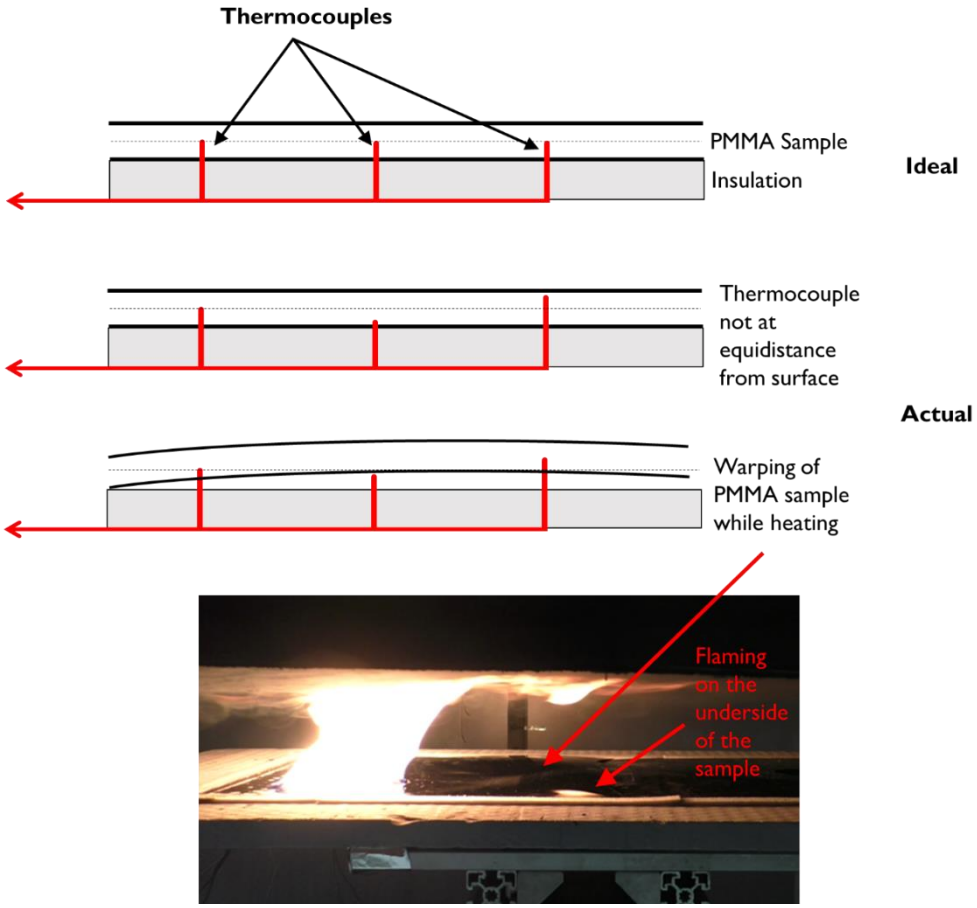


*Figure 30 Limitations of temperature measurements*

## 3.5 GAS-PHASE TEMPERATURE MEASUREMENTS

Other than the surface temperature, the temperature of the gap was also measured in order to investigate its contribution to the heat transfer process driving flame spread. Similar to the method used for calculation of PMMA temperatures, the average temperature over 5 cm was obtained and plotted. Figure 31 shows how the gas temperatures within the gap between the panels and the sample develops as the flame propagate along the sample for tests with gap distances H = 25 cm and H = 20 cm. Due to the lower rate of entrainment into a plume hindered by the panel than a vertical plume, gas temperatures are higher since the mixing between the hot gas layer and the cooler entrained air is inefficient. This accounts for the difference in the gas layer temperatures between H = 25 cm and H = 20 cm. Tg4-6 show similar trends to Tg1-3 for both tests in terms of changes of temperature with distance away from the flame. This gas layer and its heating effect on the panel contribute to the higher surface temperatures of the sample compared to the free burning case. However, as these temperatures decrease away from the fire, its effect on pre-heating is limited to the sample ahead of the flame front. The plots show that although the effect on spread rate is minimal,

the gas temperatures are increased significantly when the gap distance reduces from 25 cm to 20 cm. This increase in gas temperatures within the gap could assist in understanding the growth phase for lower gap distances.

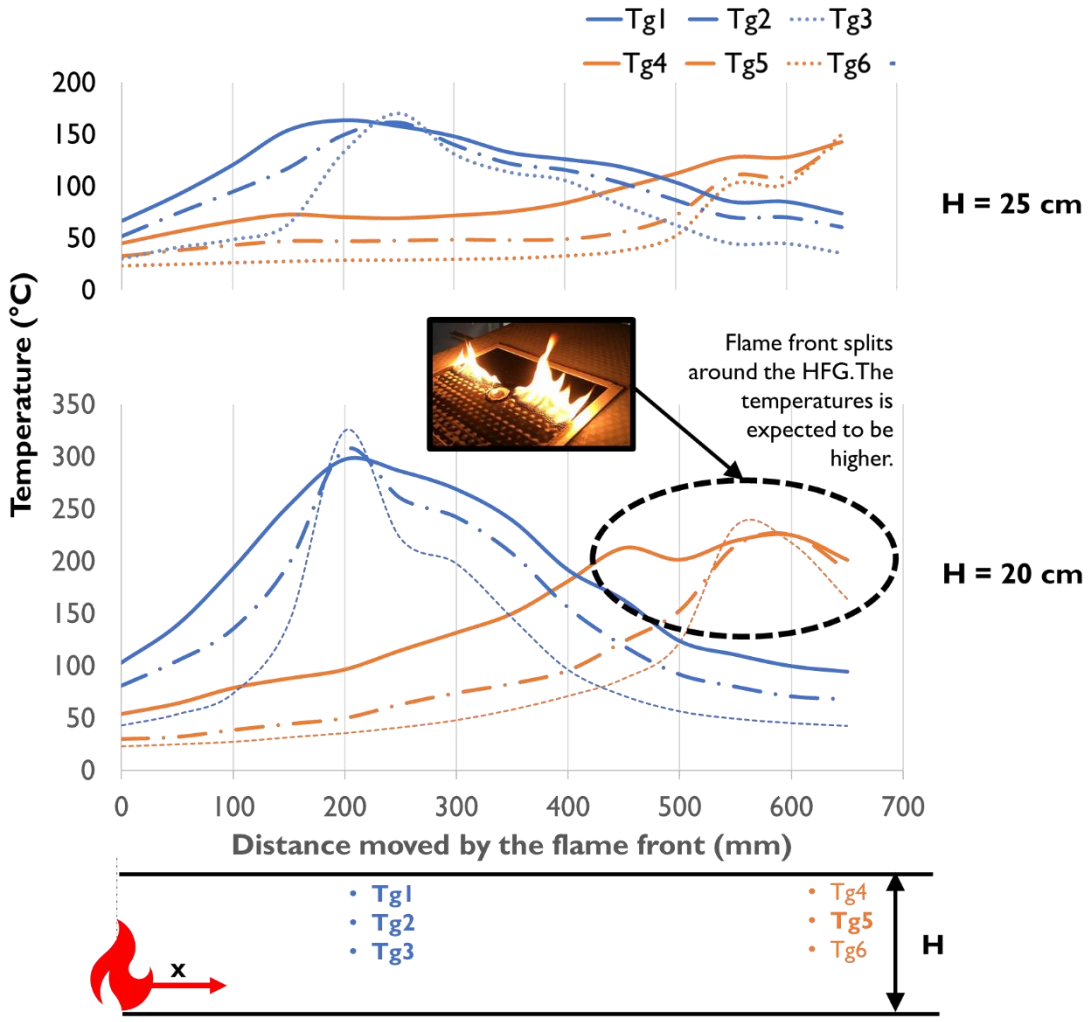


*Figure 31 Gas temperatures in the gap between the panel and sample for test 2 and 3*

For gap distances < 17 cm, gas temperatures profiles vary as the fire goes through the various stages of growth as explained. Figure 32 shows the gas temperature profile for H = 10 cm that shall be used for further discussion as the thermocouples measuring the gas phase would be closer to the sample. Tests with H=15 cm and H=17 cm shows similar trends to H = 10 cm. During the growth phase, the temperature increases as the fire spreads towards the thermocouples but at a faster rate compared to H = 20 cm. At 10 cm away from Tg1, the temperature already reached 300 °C (which is the maximum temperature when H = 20 cm) and continues to increase. From the understanding that the fire is growing within this stage and that the temperatures are significantly higher, it can be inferred that the energy released by the fire is not sufficiently loss to the surroundings causing the fire to grow further until

the fire produces flames which are large enough to deflect under the panel. At the onset of the accelerated phase as characterised by flame deflection on the panel, there is a rapid increase in temperature of the gases even for Tc6 which is located only 2 cm above the sample surface. This has an effect of reducing the heat loss from the sample to the surroundings and fire spread becomes rapid.

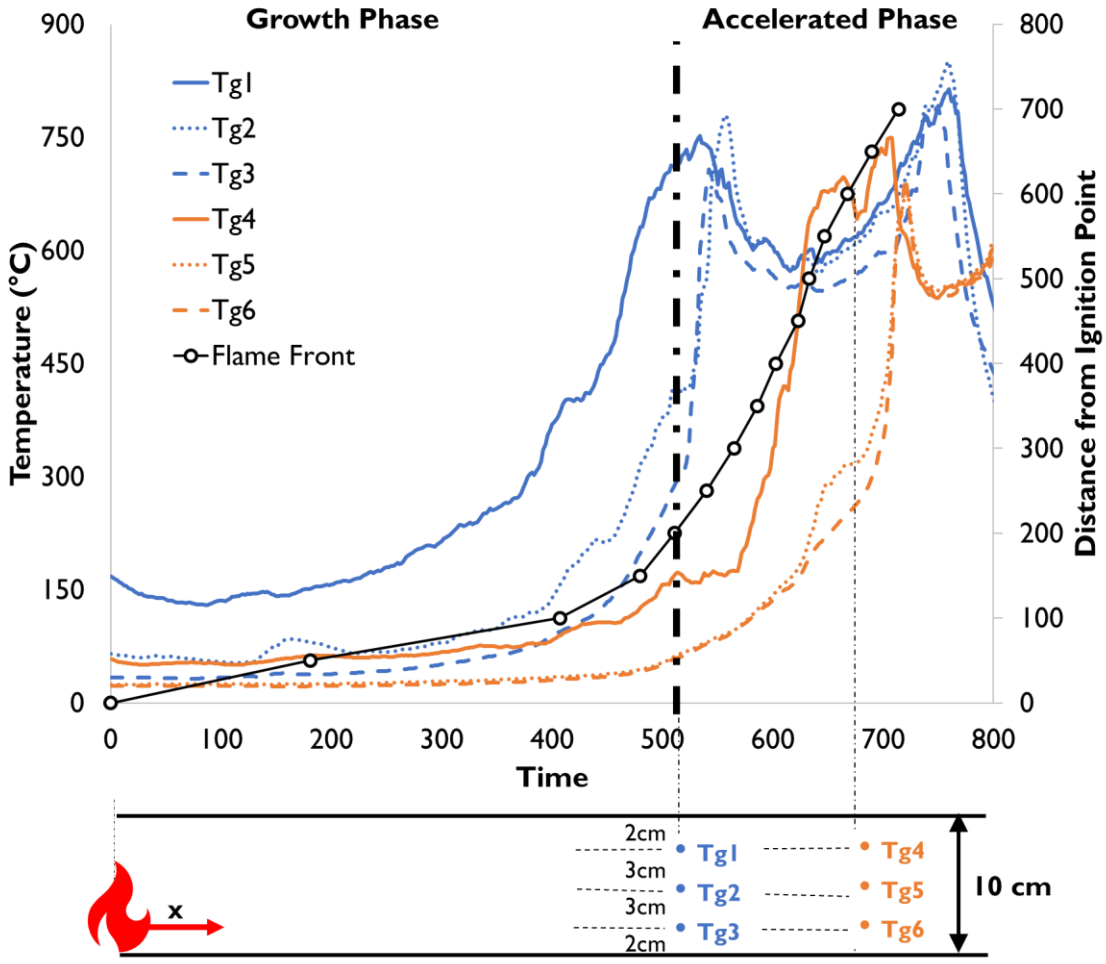


*Figure 32 Gas temperature profiles for Test 6 (H = 10 cm)*

In order to have a comparison with the steady state case, Figure 33 shows the gas temperatures at mid-plane of configurations as a function of distance travelled by the flame front. It can be seen that rapid increases in temperatures are seen after the onset of deflection under the panel with temperatures reaching more than 200 °C when the measurement point is 150 mm from the fire for Test 4-6 (i.e. H = 17 cm, H = 15 cm and H = 10 cm) compared to H = 20 cm. Given that for these tests, the midplane is closer to the sample, these high temperatures significantly contribute to the flame spread resulting in accelerated flame spread.

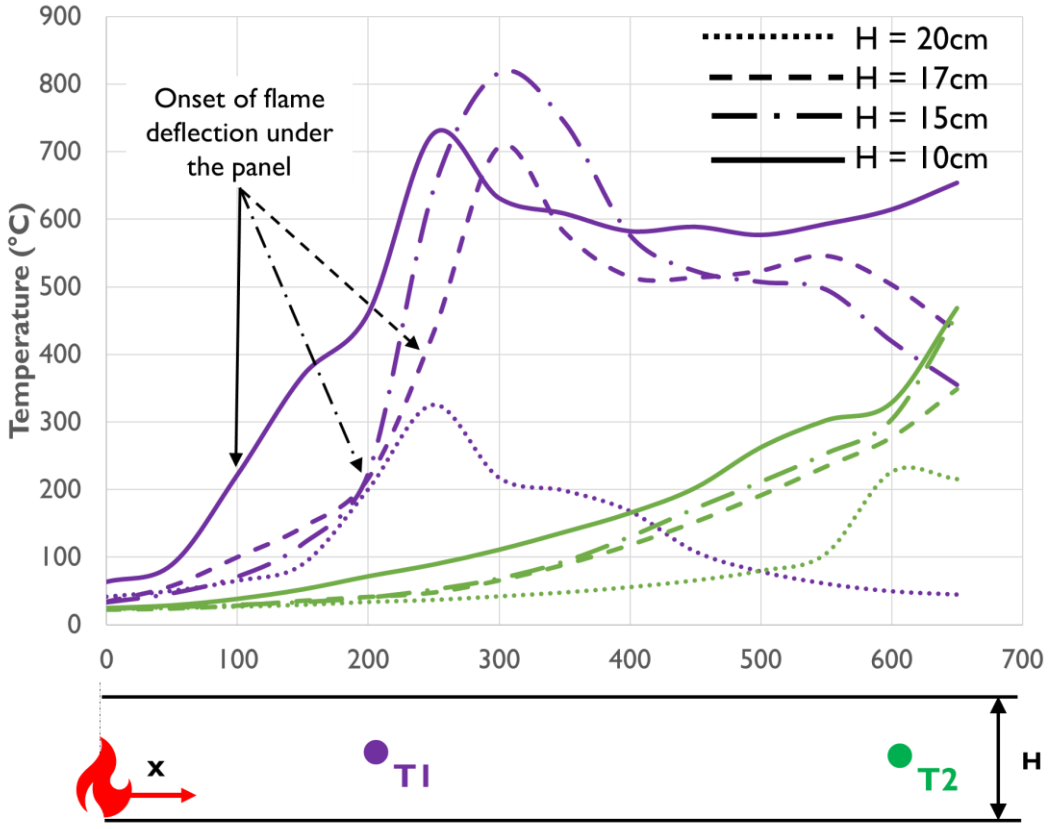


*Figure 33 Comparison of gas temperatures at midplane of the gap*

### 3.5.1 Limitations of measurements

The use of thermocouples for gas-phase temperatures in this set-up would lead to possible inaccuracies of the readings, Sources of systematics error would be due to radiation from the flames as well as radiation from the panel which is followed by convective loss to the surrounding temperatures. This could lead to lower temperatures being recorded by the thermocouples. However, an observable trend is sufficient for the purpose of these test without the need to obtain absolute data.

## 3.6 Measurements of Radiant Heat Flux

The radiative heat flux measured by the heat flux gauge would be able to quantify the resultant radiative heat flux due to the panel. The heat flux measured was averaged over 5 cm of distance moved by the flame front in order to obtain the plot shown in Figure 34.

For the test without the panel, the radiative heat flux would be solely from the radiation on the flame incident on the sample. However, with the presence of the panel at H = 25 cm and H = 20 cm, the radiative heat flux increased due to radiation from the hot gases and the heated panel. It can also be seen that the radiative heat flux extends to the same distance as

the pre-heated length shown in Figure 29. At these gap distances, the increase in heat flux is minimal with its effects is limited to the pre-heated length of 200 – 300 mm away from the flame front. Although the measurements were only taken at a single point, with reference to the convergence in surface temperature ahead of the flame as shown in Figure 29, it can be deduced that the heat flux distribution ahead of the flame is constant as the flame propagates, resulting in the steady flame spread rate observed.

However, for tests with H = 17 cm, 15 cm and 10 cm, a rapid increase in radiative heat flux upon the flame deflection under the panel was observed. Although this occurs earlier in the flame propagation for H = 10 cm, the heat flux distribution for these three tests eventually converge which suggests that the heat flux distribution for all three tests would tend towards a similar profile. The discrepancies in the data for H = 10 cm could be attributed to experimental error that would be explained in Section 3.6.1 as it would be expected that the imposed heat flux near the flame front would be similar or even higher than H = 15 cm. This convergence of radiative heat flux profiles coincides with the point where the deflected flames extend such that they were directly above the heat flux gauge. From Figure 22, Figure 23 and Figure 24, the point where flame extension, $L_E$ is above the heat flux gauge i.e. 550 mm away from the ignition point, coincides with the position of the flame front at 300 – 350 mm which is 200 - 250 mm away from the heat flux gauge. Thus, it can be deduced that once flames have deflected above the surface, the radiative heat flux incident on the surface is independent of the gap distance which supports the earlier observation that flame spread rate after deflection tend towards an identical constant flame spread rate.

These findings concur with experiments carried out by Kristensen et. al. measuring received heat flux from a gas burner at a nearby surface with the influence of a PV panel [9]. Kristensen et. al. concluded that incident heat flux due to flame deflection is dominant compared to re-radiation from the PV panel. This was demonstrated in the current study supported by the resultant effect on flame spread. Higher measured radiative heat fluxes upon flame deflection were recorded for tests with H = 17 cm, 15 cm and 10 cm compared to tests with H = 25 cm and 20 cm where there is no deflection of flames and incident radiation was from the heated panel. In this study, these observations were further explored in terms of its effect on flame propagation rate and differing flame spread rates were observed as radiation from deflected flames would give rise to accelerated flame spread rates while re-radiation from heated panels would only increase the flame spread rate slightly compared to the free burning scenario.

From the radiative heat flux data, there is a stark increased in imposed radiative heat flux when the gap distance reduces below 20 cm. Further reduction in the gap distance did not have a significant influence on the radiative heat flux imposed on the sample. This show the importance in establishing a critical gap distance in order to ensure that there is no thermal runaway caused by the increased heat flux imposed by the deflected flame.

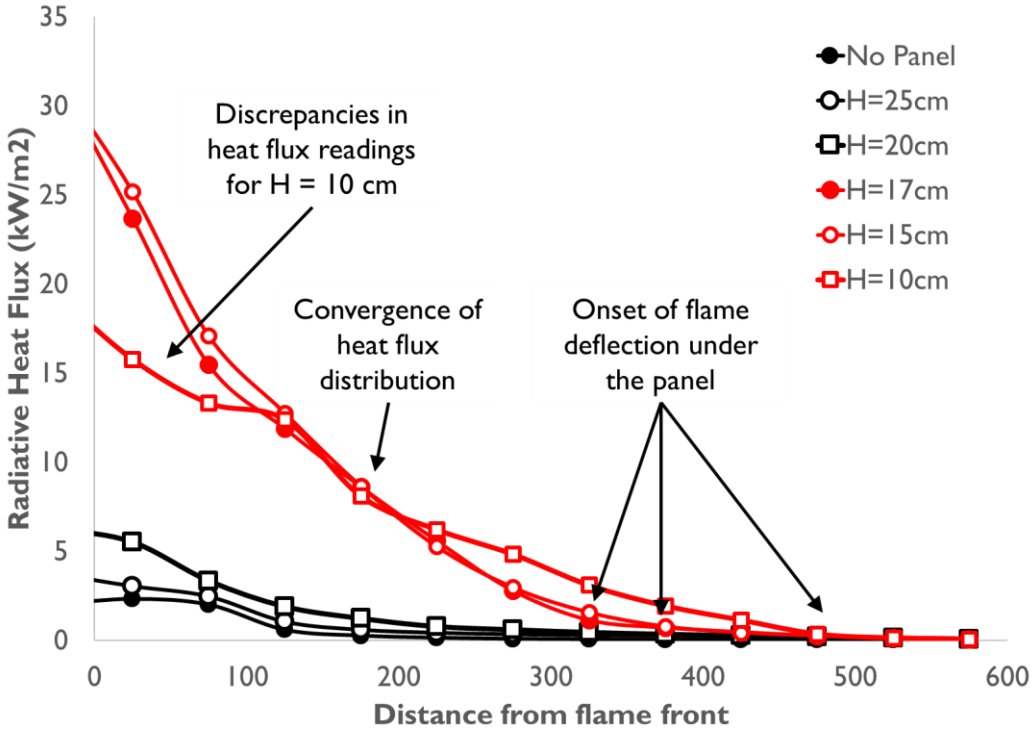


*Figure 34 Radiative heat flux over distance away from the flame front*

### 3.6.1 Limitations of measurements

Although the trends could be observed, measurement errors from the set-up should be considered. A sharp peak when the flame front reaches the heat flux gauge is expected. However, this was not observed due to the splitting of the flame front around the heat flux gauge. As the pyrolysis length is not sufficient to engulf the heat flux gauge, the heat flux received by the gauge is reduced. It was also expected that the heat flux gauge when H=10 cm should measure higher values. The reason for this could be attributed to the warping of the PMMA sample around the heat flux gauge that could shield it from incoming radiation.

Furthermore, the quartz disc placed on the heat flux gauge to shield it from convective heat transfer as well as protect the heat flux gauge from damage could affect the reliability of the measurements. This is especially so as the heat flux gauge has not been calibrated with the quartz disc. As the sensing element not be placed along the same plane as the sample, a distorted view angle will affect the radiation reading. The use of quartz disc as a window

distorts the view angle and the spectral response of the heat flux gauge by absorbing a significant amount of radiation [38]. Thus, calibration of the heat flux gauge with the window should be carried out.

Furthermore, the current set-up did not facilitate the replacement of heat flux gauge based on the expected range of heat flux from the experiment. This could lead to uncertainties especially at high heat flux values exceeding the rated value of the gauge which could account for the unexpectedly low heat flux readings near the flame for H = 10 cm. Selection of the heat flux gauge and facilitating the replacement of heat flux gauge according to the experiment could assist in obtaining more accurate values of heat flux.

## 3.7 Energy Balance for Flame Spread

Experimental results have shown that a critical gap distance exists whereby the flame spread characteristics changes. Although based on the experimental set-up this has been determined to be between 17 cm and 20 cm, an understanding on the conditions that govern that transition would assist in forming a generalised knowledge that could assist in predicting the critical gap distance in other scenarios. An analysis of the energy balance was attempted to form this understanding

Energy balances constructed through experimental measurements of temperatures and radiant heat flux are a direct method for analysing the relative magnitude of the different heat transfer mechanisms driving flame spread. The fundamental equation (1) shall be used to derive a heat transfer model for flame spread. Given a thermally thin material, the heat transfer equation can be represented as:

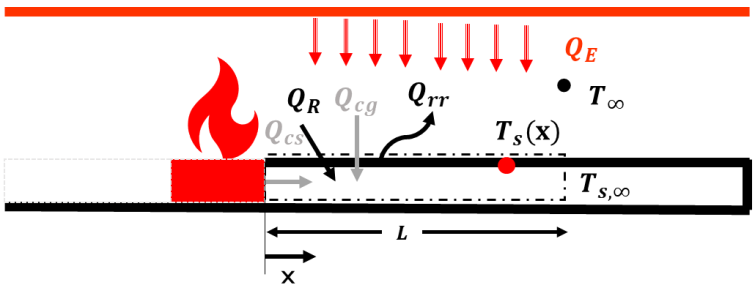


*Figure 35 Diagram for heat balance calculations*

$$\rho v c_p (T_p - T_{s,\infty})\delta = \dot{q}^{"} L$$

| | | | | |
|---|---|---|---|---|
| Where ρ | = | density of PMMA | = | 1190 kg/m³ |
| $c_p$ | = | specific heat capacity of PMMA | = | 2.09 kJ/kgK |
| $T_p$ | = | pyrolysis temperature of PMMA | = | 250 |
| $T_{s,\infty}$ | = | initial temperature of PMMA | | |
| $\delta$ | = | thickness of sample | = | 2 mm |
| L | = | pre-heated length | | |

Although specific heat capacity of PMMA varies with temperature i.e. $c_p = -0.247 + 5.69 \times 10^{-3} T$ kJ/kgK [39], an average value of 2.09 kJ/kgK shall be used as it is obtained for the temperature range of 20°C to 363°C which is within the temperature range of PMMA in our experiments [40]. The pyrolysis temperature from experimental data as shown in Figure 25 is 225°C. However, to account for the lag in thermocouple readings, a higher pyrolysis temperature should be expected and the value of 278°C is selected[9] [41].

In order to explain the changes in flame spread rate as the panel is introduced and the gap distances are reduced, this equation will be used to study the steady state case and review the trends in order to gain an understanding on the conditions leading to a changed flame spread characteristic. Thus, the left side of the equation was resolved into the different heat transfer mechanisms as shown in Figure 2 and compared with experimental data where

$$\dot{q}^{"} L = Q_{cs}{}' + Q_{cg}{}' + Q_R{}' + Q_E{}' - Q_{rr}{}'$$

Based on experiments on horizontal fire spread on PMMA, radiative heat transfer has been identified as the dominant mode of heat transfer driving the flame spread [19]. Furthermore, effects of the panel have shown to induce an additional radiative heat flux on the sample ahead of the flame front that increases flame spread rate. Thus, it is assumed that the flame spread is driven primarily by radiative heat transfer. The above equation reduces to:

$$\dot{q}^{"} L = \ Q_T{}' = Q_R{}' + Q_E{}' - Q_{rr}{}'$$

[9] This value is based on measured values for opposed-flow flame spread on 1.59 mm PMMA Polycast. The sample used in our experiment is 2 mm thick extruded PMMA. Ideally, a cone calorimeter test on the sample should be carried out to determine the actual pyrolysis temperature. However, the value of 278°C is determined to be sufficient as a reference value.

Experimentally, $Q_R{}' + Q_E{}'$ would be captured by the radiative heat flux readings of the heat flux gauge. Thus,

$$Q_R{}' + Q_E{}' = \int_{\infty}^{x} F\, dx$$

where F = heat flux gauge readings (W/m$^2$)

Re-radiated heat from the PMMA surface $Q_{rr}{}'$ can be obtained from measurement readings as such:

$$Q_{rr}{}' = \int_{\infty}^{x} \epsilon\sigma(T_S^4 - T_\infty^4)\, dx$$

where $\epsilon$ = 1 (assume blackbody as PMMA surface is black)
$\sigma$ = 5.67 x 10$^{-8}$ W/m$^2$K
$T_S$ = surface temperatures measured from thermocouples
$T_\infty$ = ambient temperature (18°C)

$T_S$ values are obtained from thermocouple readings of Ts8 as the flame propagates towards it such that surface temperature readings for maximum pre-heating temperatures could be obtained i.e. L = 500 mm. $T_\infty$ is assumed to be ambient although tests with the panels should consider the elevated gap temperatures. However, it is assumed that temperatures around the surface of the sample would still be approximately equal to the ambient temperatures due to the flow of entrained ambient air along the surface of the PMMA towards the fire.

These equations are applied for steady state tests (no panel, H = 25 cm, H = 20 cm) to observe the changes in these heat transfer mechanisms. The distribution of heat flux fluxes ahead of the flame for these tests are shown in Figure 36. Rectangular integration was then used to calculate the total heat transfer to the sample and compared with the energy required to ignite the sample as shown in Table 6.

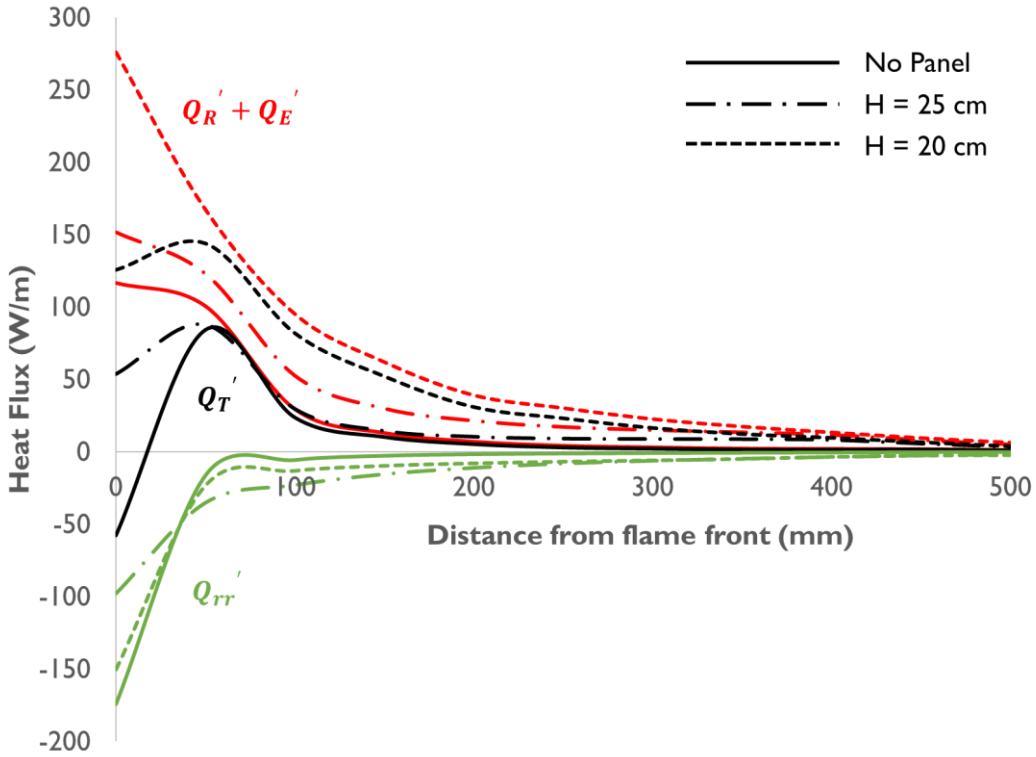


*Figure 36 Distribution of heat fluxes ahead of the flame*

*Table 6 Comparison of energy required for ignition and heat transfer to the sample*

| | $v$ (mm/s) | $T_{s,\infty}$ (°C) | $\rho v c_p (T_p - T_{s,\infty})\delta$ (W/m) | $Q_R' + Q_E'$ (W/m) | $Q_{rr}'$ (W/m) | $Q_T'$ (W/m) | $\Delta$ (W/m) |
|---|---|---|---|---|---|---|---|
| No Panel | 0.13 | 18 | **168** | 275 | 204 | **76** | **-92** |
| H = 25 cm | 0.15 | 24 | **189** | 450 | 209 | **240** | **51** |
| H = 20 cm | 0.20 | 26 | **250** | 740 | 232 | **540** | **290** |

From Figure 36, for the tests with no panel, it can be seen that $Q_R' + Q_E'$ within 50 mm from the flame front is lower than expected due to the flame front splitting as explained in Section 3.6.1. This results in the net heat transfer being less than the energy required for flame propagation. It was observed that the total incident radiative heat flux almost doubled with the introduction of the panel at H = 25 cm although the heat losses by re-radiation from the surface remains constant. This increase in net heat transfer to the surface resulted in an increase in the constant flame spread rate. Since the $Q_R' + Q_E'$ profile for H = 20 cm especially at 50 mm away from the fuel surface seems to be more accurate, this shall be used for discussion. There is a significant difference between the heat needed to ignite the control

volume and the heat transferred to the control volume. This difference could be attributed to the experimental errors and the assumptions made in this analysis. However, it also highlights the potential presence of another mechanism of heat loss from the surface in order to maintain the balance between heat loss from the surface and the heat incident on the surface that will result in a constant flame spread rate. This could be attributed to the convective losses along the surface of the sample. The convection current could assist in dissipating heat from the surface in order to maintain the heat balance for a constant flame spread though the influence of convection/conduction in the gas phase was not studied in this experiment. Thus, the attempt at establishing the energy balance for flame spread is inconclusive.

The experimental study also revealed the impact on fire growth due to the presence of the panel providing thermal feedback. Thus, energy balance considering the whole system should be considered although the measurement points such as heat release rate are not available in this study. Figure 37 shows a conceptual energy balance diagram to form an understanding on how thermal balances within the system could lead to fire growth. Based on the mass loss rate data as well as observations of the pyrolysis length and flame height, the presence of the panel and lower gap distance has an effect of enhancing the heat release rate of the fire. However, steady state situations can still be reached if the heat could be sufficiently loss to the surroundings, the panel and the sample ahead of the flames. An understanding of these heat loss mechanisms and how it is affected by gap distances would be able to reveal the conditions determining the critical gap distance.

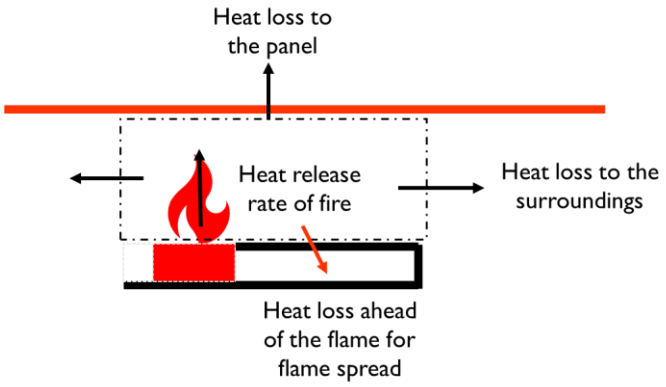


*Figure 37 Conceptual energy balance diagram for the system*

## 3.8 EXPERIMENTS WITH ACTUAL PV PANELS

In order to analyse if the results are reproducible with actual PV panels, 3 tests were conducted by replacing the PV surrogate with an actual PV panel. The selected PV Panel is the SolarWorld SunPanel Plus SW Poly 250. It is made of poly-crystalline cells with a 4 mm tempered glass on the front and polymer back sheet encasing the cells. The panel is framed by clear anodized aluminium. Based on the findings from the previous tests with the surrogate panel, the heights of 20 cm, 17 cm and 15 cm were conducted to compare whether the trends observed with the surrogate panel where the fire spread behaviour changes as the gap height changes from 20 cm to 17 cm is applicable when the PV panel was installed instead.

The configuration of the experiment is changed slightly as the underside of the panel was not flat. The notch created by the edges of the panel would lead to stagnation of gases underneath the panel. The thermocouple used for gas temperatures are re-configured to study the temperatures within this gas layer. Thus, the modification made are shown in Figure 38. It should be noted that the ignition fuel was changed to Hexane for the test of H = 17 cm as there was insufficient methanol. This may cause a deviation of results for the experiment of H = 17 cm.

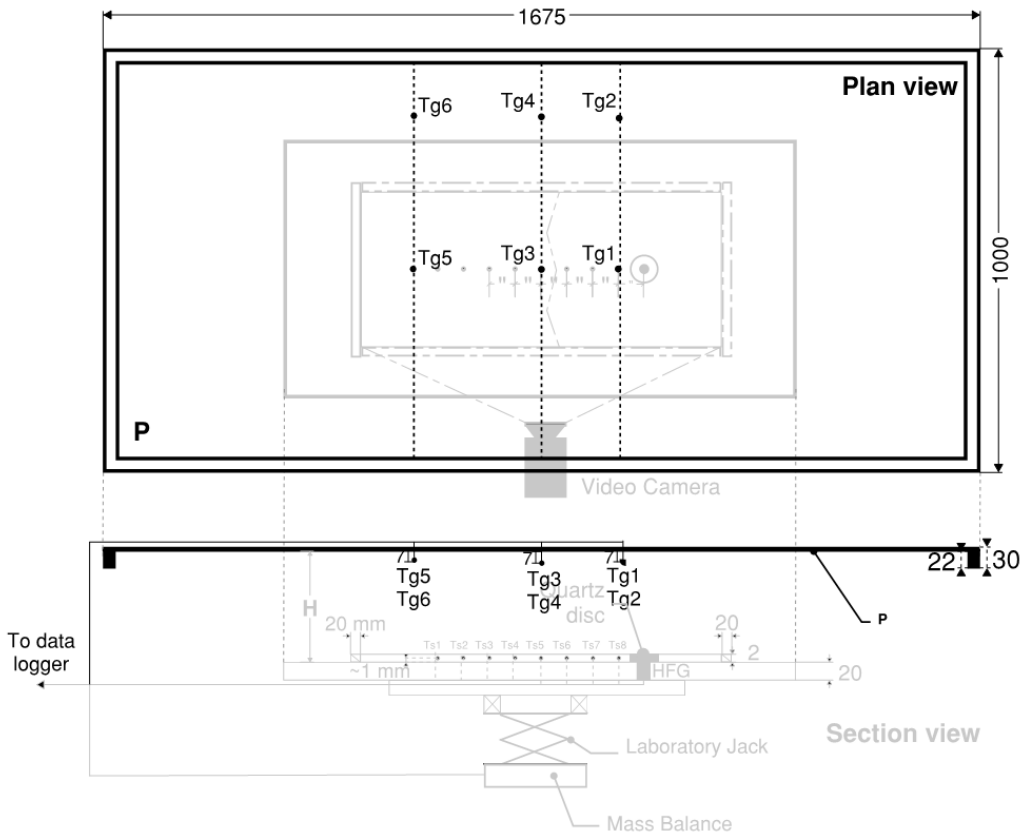


*Figure 38 Modification to set-up for tests with PV panels*

### 3.8.1 **Visual Observations**

There is no observable difference between the flame propagation characteristics when the PV surrogate was replaced by the PV panel for gap distances of 20 cm, 17 cm and 15 cm. For tests with H = 20 cm, a similar steady state was observed with flames propagating at a constant rate after a short growth and constant flame height and pyrolysis length was observed visually. Figure 39 shows the similarities in observable flame characteristics when the PV surrogate was replaced by the PV panel.

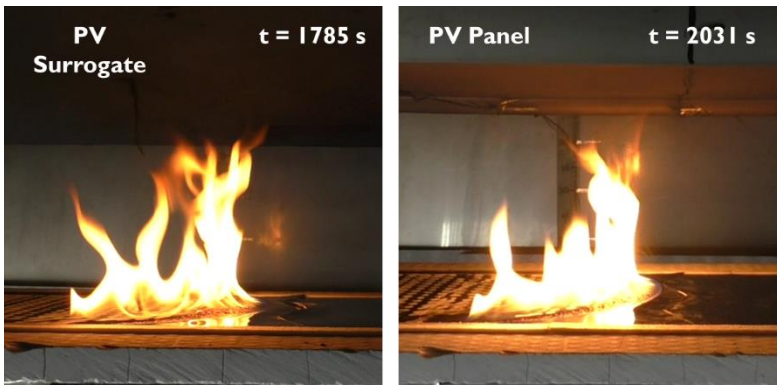


*Figure 39 Similar observations for H = 20 cm when flames reach mid-point of the sample*

Similarly, for H = 17 cm and 15 cm, both test with PV surrogate and PV panel showed a distinct growth stage with a transition to the accelerated stage upon the onset of flame deflection. The point in time and position along the sample that this occurred during the flame propagation was similar for both tests as shown in Figure 40. Flame spread for the test of H = 17 cm was faster. This could be attributed to the change in ignition fuel. However, in general, there is no significant difference in the effect of the material of the panel on the flame spread characteristics within the gap.

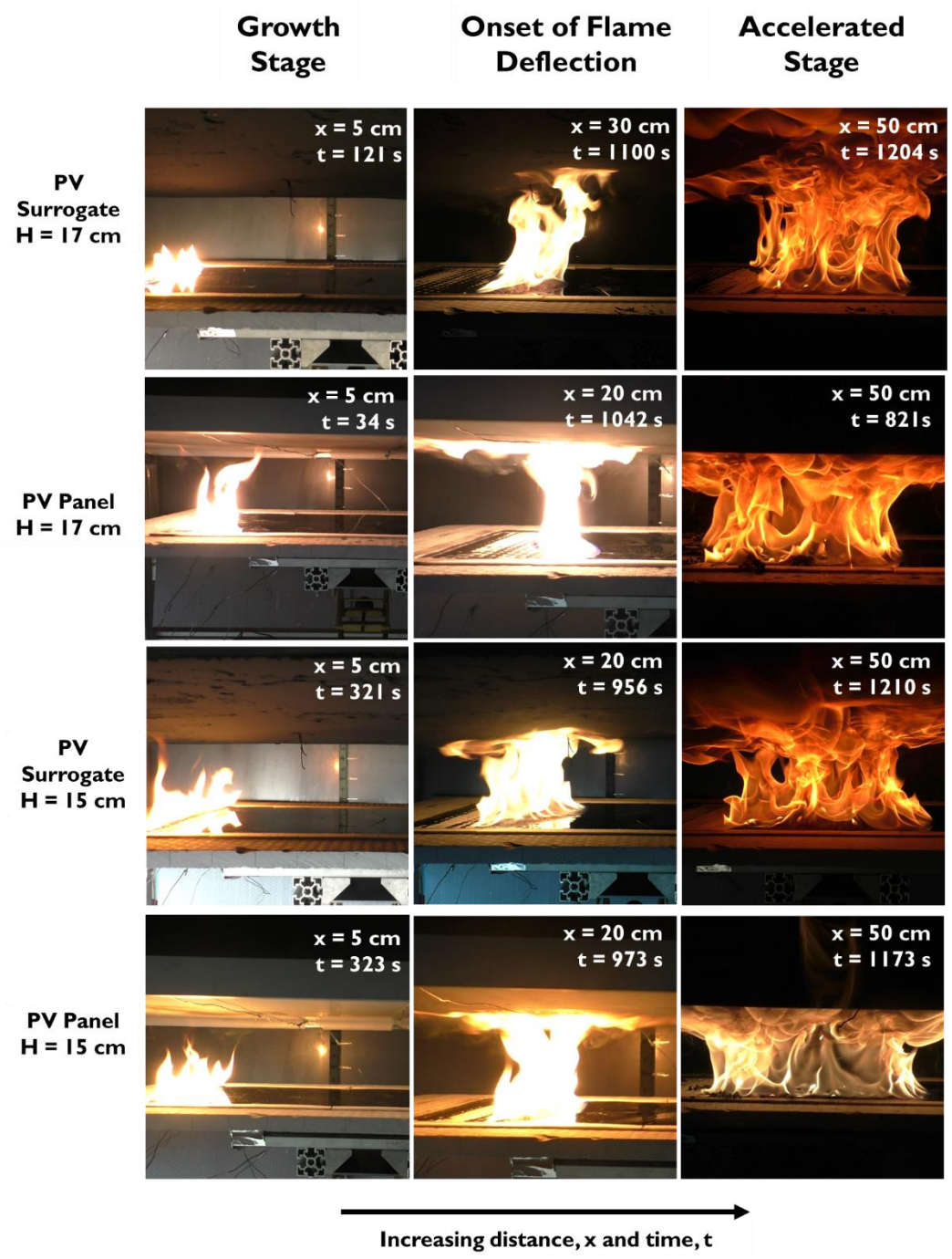


*Figure 40 Similar observations for H = 15 cm & H = 17 cm*

However, the experiment showed that the selected PV panel for our experiment is combustible under the conditions of our set-up. When gap distances were at 17 cm and 15 cm, the back sheet as well as the PV cells disintegrated when the flames deflect on the underside of the PV panel. This resulted in debris collected on the sample set-up after the experiment is completed as shown in Figure 41. Thus, the earlier assumption that PV panels were not combustible did not hold true although there is no observable impact on the general

flame spread behaviour and the flame spread rate. Furthermore, due to the deposition of debris on the PMMA sample set-up which is mounted on the mass balance as well as on the heat flux gauge, mass loss data and heat flux data may be erroneous. A summary of these measurements is found in Appendix 4.

*Figure 41 Debris from combustible panel on the sample set-up*

Observations were also made on the resultant damage on the PV panel after both experiments as shown in Figure 42. Even though there is no significant damage for the experiment with gap distance of 20 cm, there is soot deposited on the underside of the panel which suggest that the combustion efficiency is low. For the experiment with PV panel at gap distance of 15 cm and 17 cm, the damage on the panel is evident although there was no burn through of the tempered glass covering. There was also more soot deposited than the experiment with H = 20 cm which indicates that the combustion efficiency is lower with reduced gap height. This is expected as a shorter gap distance reduces the height of the plume and there is less air entrained for burning. As this could be a factor affecting the change in flame spread behaviour between the two regimes i.e. above 20 cm and below 17 cm, flame spread in oxygen deprived environments should be studied.

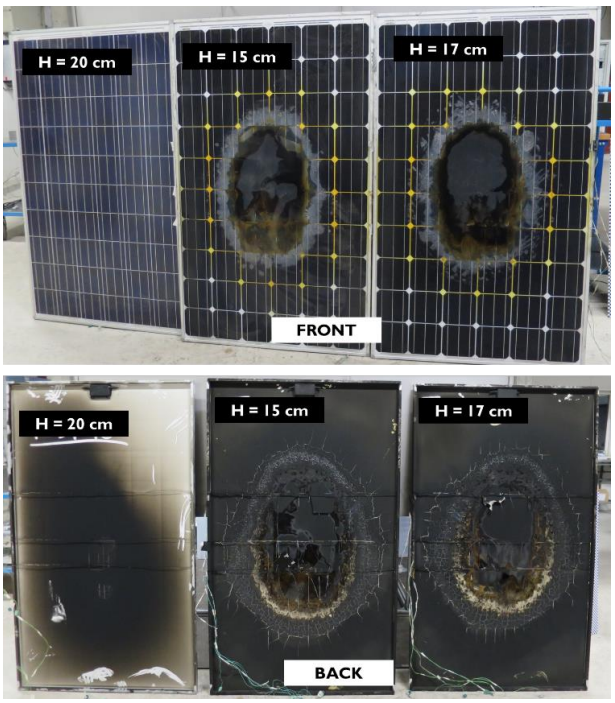


*Figure 42 PV panels after the experiment*

### 3.8.2 **Flame Spread Rate, Flame Height & Pyrolysis Zone**

The flame spread rate was compared between experiments with the PV surrogate and the PV panel as shown in Figure 43. A constant flame spread rate was achieved for H = 20 cm with the PV panel, but the flame spread rate of 0.18 mm/s was lower than 0.20 mm/s with the PV surrogate. This could be attributed to the emissivity of the back face of the PV panel since the PV surrogate panel was painted black while the PV panel had a white backing. At H = 20 cm, pre-heating of the sample ahead of the flame front is due to the hot gases on the underside of the panel which both radiates and heats up the adjacent panel which would also radiate the heat back itself to the sample. Thus, the black surface of the PV surrogate would be able to radiate more heat than the white backing of the PV panel resulting in increased radiative heat flux on the sample to pre-heat the sample further for faster flame spread. However, the difference in flame spread rate of 0.02 mm/s could be considered as negligible. At gap distance of H = 15 cm and H = 17 cm, identical behaviour in flame spread was observed for both tests with the transition from growth stage to accelerated stage occurring at the same instant and tending towards the same asymptote in the accelerated stage. However, since the ignition fuel for H = 17 cm was replaced with Hexane, the onset of flame impingement under the panel occurs earlier. Hexane has a higher heat of combustion than methanol and would result in a higher heat released when ignited. This shows that the experiment is sensitive to the ignition fuel though general trends remain similar i.e. a distinct growth and accelerated phase was observed. Thus, the experimental set-up with the PV

surrogate would be able to predict the flame spread behaviour especially in terms of determining the critical gap distance for an installation with an actual PV panel.

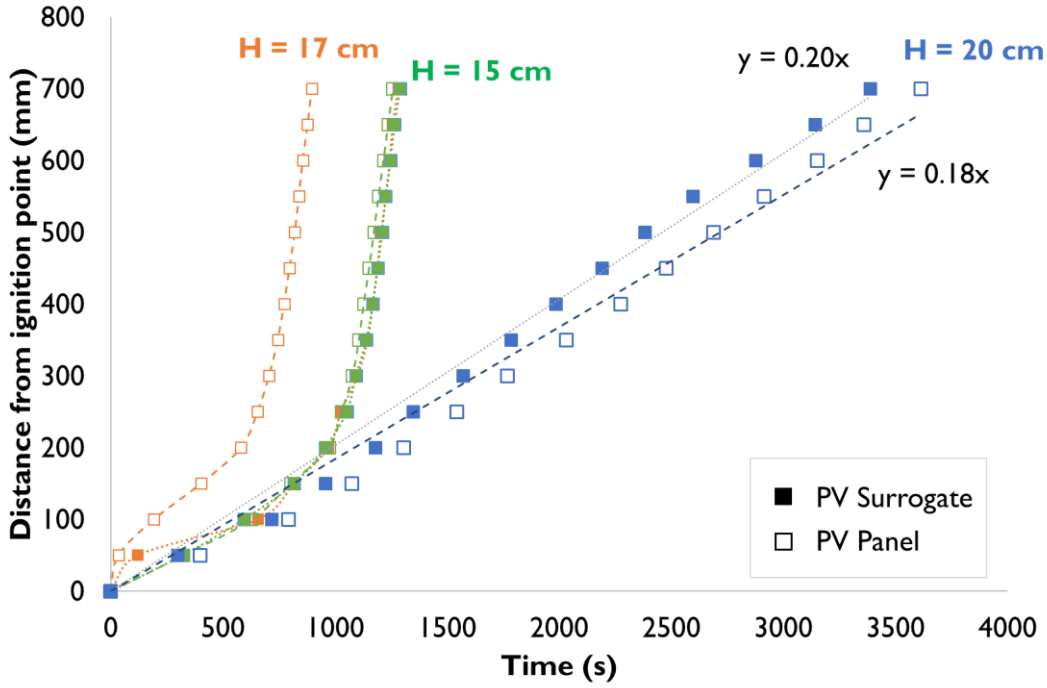


*Figure 43 Progress of the flame front over time*

# 4 CONCLUSION

An experimental study was carried out to investigate the effects of gap distance between photovoltaic installations and flat roof construction on flame spread through a simplified configuration of horizontal panel installation parallel to the flat roofs. The experiment was designed to investigate fire spread behaviour due to the presence of the panel at various gap distances. The experimental set-up consisted of a 30 cm wide thin PMMA sheets as a surrogate for combustible roofing material and a stainless-steel sheet for an incombustible panel with the distance between them varied.

The experiments revealed that there is a critical gap distance that could distinguish whether PV installations on roof would pose a significant additional fire risk compared to an open roof. Two types of flame spread behaviour could be characterised depending on whether the gap distance was above or below the critical gap distance. For the experimental set-up and materials used in this study, this critical gap distance has been found to be 17 - 20 cm.

For gap distances above 20 cm, the flame propagation was similar characteristics compared to a free burning situation with a constant flame spread rates of 0.15 – 0.20 mm/s and constant heat release rate which is comparable to a free burning scenario. The flame spread behaviour is typical of a horizontal opposed-flow flame spread which indicates that the presence of the panel is insignificant to the flame spread. Thus, PV panels installed above the critical gap distance will not pose a significant additional fire risk to existing roof construction.

For gap distances below 17 cm, flame propagation is similar to a free burning situation initially, but the fire slowly grew until the flame impinged on the panel and deflected. This initiated a rapid acceleration to a resultant flame spread rate (and heat release rate) that was more than 10 times the flame spread rate in a free burning scenario. The resultant flame spread behaviour was typical of an upward concurrent flow flame spread instead of a typical horizontal opposed flow flame spread as observed for gap distances above 20 cm. This indicates that the flame spread dynamics changed due to the presence of the panel (compared to a free burning scenario).

These observations indicate that PV panels installed below the critical gap distance pose a threat to the rooftop construction as a small fire within the gap has the potential to grow to a significant fire with rapid flame spread that could be hard to control. Thus, PV panels installed below the critical gap distance will pose a significant fire risk to the existing roof construction.

These findings highlight the need to consider critical gap distances for PV panels on roofs and thus also in test procedures used for fire classification purposes. Current pass-fail criteria based on maximum spread distance within a time interval might under estimate the resultant risk posed by the PV installations especially if the installations are below the critical gap distance. Acceptance criteria for these classification tests must be reviewed by taking into account the flame spread behaviour throughout the tests and determine if there is a tendency towards an accelerated flame spread. Thus, this study has revealed the need to review current test procedures used in classification of PV installation on roofs.

Determining the critical gap distance for a generalised scenario would assist in formulating guidelines in the design for PV installations on roofs. An analysis of the energy balance for flame spread was attempted based on experimental data to better understand the changes in heat transfer mechanisms as the gap distances decreases. However, due to the assumptions made and limitations in the experimental measurements, the outcomes of the analysis are inconclusive. Furthermore, the flame spread behaviour highlights the need to establish an understanding on the energy balance as a system considering heat loses to the surroundings though this is not covered in the current study. Thus, this study has revealed a need for a more thorough analysis in order to obtain a critical gap distance for generalised application.

Still, the current experimental set-up using a PV surrogate was able to provide a close indicator of the flame spread behaviour for actual PV panels. Based on the tests with the actual PV panel, there are agreements on the critical gap distance with the tests with PV surrogate. Considering that the PV panel disintegrate when burnt and cannot be re-used, the current experimental set-up could be a potential test set-up for determining gap distances.

In summary, the current study demonstrated that flame propagation within the gap between PV installations and flat roofs are strongly affected by minute differences in the gap height. Based on the experimental set-up in this study, reducing the gap distance from 20 cm to 17 cm could lead to a significant difference in flame spread behaviour. There is a critical gap height above which the risk of extended damage is low though further investigation is required to determine the actual critical gap for different scenarios. The critical gap could be used as a mitigation measure against extensive fire spread on roofs. Hence, a critical gap for fire safety should also be factored in PV installation design in conjunction with other drivers such as wind uplift and seismic effects in order to minimise the extensive damage on roofs housing PV installations in the event of a fire.

## 4.1 FUTURE WORK

Although the findings using actual PV panels from this experimental study have been positive, enhancements could be made in order to further validate its applicability to actual installations by using actual roofing membrane as the sample. The experiments carried out in this study are based on PMMA as a surrogate material for roof insulation. However, the conditions may differ for other materials with different thermal properties as seen from the fundamental equations for flame spread. Furthermore, assumptions of the sample being thermally thin may not be applicable for roofing materials which are typically thermally thick in order to function as an insulator. As the thickness increased, flame spread behaviour is expected to change. Thus, the experimental set-up should be developed further in order to evaluate the effect of thermal thickness of the material on the critical gap height.

Given that roofs are exposed to environmental effects such as wind, imposed airflow due to wind should also be considered. Such induced airflow by wind could exacerbate the flame spread even when there is no flame deflection under the panel as the wind will cause the flame to bend over the surface, intensifying radiative heat flux that will exacerbate the flame spread. Thus, further studies on the effect of a wind-driven flame spread and the applicability of a critical gap distance for such situations should be further analysed.

Although this experimental study investigates impact of gap distances in horizontal gaps, PV installations are also typically installed at inclined angles from the flat roof surface. This could vary the fire dynamics within the gap between the PV installation and the flat roof and could render the concept of a critical vertical gap irrelevant for such installations. Thus, further studies on fire spread between the roof and inclined surfaces should be studied to determine whether gap distances would still be critical or whether inclination angles would have an impact on the fire spread behaviour.

The outcome of this study was able to identify the presence of a critical gap distance, but further work has to be done to gain an understanding on how this critical distance could be predicted. This may require adjustment on the experimental set up such that the models could be validated with experimental data. This would be useful in establishing guidelines on the required installation gap in order to reduce fire risk of PV installations on flat roofing.

# 5 REFERENCES


[1] SolarPower Europe, "Global Market Outlook For Solar Power: 2018 - 2022," 2018. [Online]. Available: http://www.solarpowereurope.org/wp-content/uploads/2018/09/Global-Market-Outlook-2018-2022.pdf. [Accessed: 20-Feb-2019].

[2] M. Motyka, A. Slaughter, and C. Amon, "Global Renewable Energy Trends," *Deloitte Insights*, 2018. [Online]. Available: https://www2.deloitte.com/insights/us/en/industry/power-and-utilities/global-renewable-energy-trends.html. [Accessed: 20-Feb-2019].

[3] Solar Energy Industries Association (SEIA), "Solar Means Business: Tracking Corporate Solar Adoption in the U.S.," 2018. [Online]. Available: http://www2.seia.org/l/139231/2018-04-18/29ls1f. [Accessed: 20-Feb-2019].

[4] S. Namikawa, "Task 12 : Photovoltaics and Firefighters' Operations : Best Practices in Selected Countries," *International Energy Agency Photovoltaic Power Systems Program*, 2017. [Online]. Available: http://www.iea-pvps.org/index.php?id=449&eID=dam_frontend_push&docID=4044. [Accessed: 20-Feb-2019].

[5] TÜV Rheinland Energie und Umwelt GmbH, "Assessing Fire Risks in Photovoltaic Systems and Developing Safety Concepts for Risk Minimization," *Energy.gov*, 2018. [Online]. Available: https://www.energy.gov/sites/prod/files/2018/10/f56/PV Fire Safety Fire Guideline_Translation_V04 20180614_FINAL.pdf. [Accessed: 20-Feb-2019].

[6] P. Cancelliere, "PV Electrical Plants Fire Risk Assessment and Mitigation According to the Italian National Fire Services Guidelines," *Fire and Materials*, vol. 40, no. 3, pp. 355–367, 2016.

[7] L. Fiorentini, L. Marmo, E. Danzi, V. Rossini, and V. Puccia, "Fire Risk Analysis of Photovoltaic Plants. A Case Study Moving From Two Large Fires: From Accident Investigation and Forensic Engineering to Fire Risk Assessment for Reconstruction and Permitting Purposes," in *Chemical Engineering Transactions*, 2014, vol. 48, pp. 427–432.

[8] R. Wills, J. A. Milke, S. Royle, and K. Steranka, *Best Practices for Commercial Roof-*

*Mounted Photovoltaic System Installation*. Springer New York, 2015.

[9] J. S. Kristensen, B. Merci, and G. Jomaas, "Fire-induced Reradiation Underneath Photovoltaic Arrays on Flat Roofs," *Fire and Materials*, vol. 42, no. 3, pp. 316–323, 2018.

[10] B. Backstrom and D. Sloan, "Effect of Rack Mounted Photovoltaic Modules on the Fire Classification Rating of Roofing Assemblies Phase 2," *Underwriters Laboratories Inc. (UL)*, 2012. [Online]. Available: http://www.solarabcs.org/current-issues/docs/UL_Report_Phase2_1-30-12.pdf. [Accessed: 20-Feb-2019].

[11] B. Backstrom and M. Tabaddor, "Effect of Rack Mounted Photovoltaic Modules on the Fire Classification Rating of Roofing Assemblies," *Underwriters Laboratories Inc. (UL)*, 2010. [Online]. Available: http://www.solarabcs.org/current-issues/docs/UL_Report_PV_Roof_Flammability_Experiments_11-30-10.pdf. [Accessed: 20-Feb-2019].

[12] B. Backstrom and M. Tabaddor, "Effect of Rack Mounted Photovoltaic Modules on the Flammability of Roofing Assemblies – Demonstration of Mitigation Concepts," *Underwriters Laboratories Inc. (UL)*, 2010. [Online]. Available: http://www.solarabcs.org/current-issues/docs/UL_Report_PV_and_Roof_Flammability_Mitigation_2-10-10.pdf. [Accessed: 20-Feb-2019].

[13] B. Backstrom and D. Sloan, "Report of Experiments of Minimum Gap and Flashing for Rack Mounted Photovoltaic Modules Phase 4," *Underwriters Laboratories Inc. (UL)*, 2012. [Online]. Available: http://www.solarabcs.org/current-issues/docs/UL_Report_Gap_and_Flashing_Exps_3-29-12.pdf. [Accessed: 20-Feb-2019].

[14] SEAOC Solar Photovoltaic Systems Committee, "Wind Design for Low-Profile Solar Photovoltaic Arrays on Flat Roofs," *Structural Engineers Association of California*, 2012. [Online]. Available: http://files.engineering.com/download.aspx?folder=7ae26414-8066-4d06-b001-198e5aaf6d88&file=2012-08_SEAOC_Solar_PV_wind_document_Final.pdf. [Accessed: 28-Apr-2019].

[15] M.-C. Hong, "A Study of the Required Spacing for Preventing Fire Spread Between Photovoltaic Arrays on Flat Roofs," Msc Thesis, IMFSE, 2018.

[16] D. Drysdale, *An Introduction to Fire Dynamics*, 3rd ed. Wiley, 2011.

[17] J. N. De Ris, "Spread of a laminar diffusion flame," *Symposium (International) on Combustion*, vol. 12, no. 1, pp. 241–252, 1969.

[18] F. A. Williams, "Mechanisms of fire spread," *Symposium (International) on Combustion*, vol. 16, no. 1, pp. 1281–1294, 1977.

[19] S. R. Ray, A. C. Fernandez-Pello, and I. Glassman, "A study of the heat transfer mechanisms in horizontal flame propagation," *Journal of Heat Transfer*, vol. 102, no. 2, pp. 357–363, 1980.

[20] J. G. Quintiere, *Fundamentals of Fire Phenomena*. John Wiley and Sons, 2006.

[21] A. C. Fernandez-Pello, "The Solid Phase," in *Combustion Fundamentals of Fire*, Academic Press Ltd., 1995, pp. 31–100.

[22] A. Fernandez-Pello, "Laminar Flame Spread Over Flat Solid Surfaces," ProQuest Dissertations Publishing, 1975.

[23] A. F. Robertson, *Fire Standards and Safety*, 614th ed. ASTM Special Technical Publication, 1976.

[24] R. L. Alpert, "Ceiling jet flows," in *SFPE Handbook of Fire Protection Engineering, Fifth Edition*, Springer New York, 2016, pp. 429–454.

[25] P. H. Thomas, "Factors affecting ignition of combustible materials and their behaviour in fire," in *International Symposium on Fire Safety of Combustible Materials*, 1975, pp. 84–99.

[26] A. C. Fernandez-Pello and F. A. Williams, "Laminar flame spread over PMMA surfaces," *Proceedings of the Combustion Institute*, vol. 15, pp. 217–231, 1974.

[27] J. G. Quintiere, *Principles of fire behavior*, 2nd ed. Boca Raton: CRC Press, Taylor & Francis Group, 2017.

[28] L. Jiang, C. H. Miller, M. J. Gollner, and J. Sun, "Sample width and thickness effects on horizontal flame spread over a thin PMMA surface," *Proceedings of the Combustion Institute*, vol. 36, no. 2, pp. 2987–2994, 2017.

[29] R. S. Magee and R. F. McAlevy, "The Mechanism of Flame Spread," *Journal of Fire and Flammbility*, vol. 2, pp. 271–297, 1971.

[30] L. Orloff, J. De Ris, and G. H. Markstein, "Upward turbulent fire spread and burning of fuel surface," *Symposium (International) on Combustion*, vol. 15, no. 1, pp. 183–192, 1975.

[31] Y. Pizzo, J. L. Consalvi, P. Querre, M. Coutin, L. Audouin, B. Porterie, and J. L. Torero, "Experimental observations on the steady-state burning rate of a vertically oriented PMMA slab," *Combustion and Flame*, vol. 152, no. 3, pp. 451–460, 2008.

[32] L. Sherwood, B. Backstorm, D. Sloan, C. Flueckiger, B. Brooks, and A. Rosenthal, "Fire Classification Rating Testing of Stand-Off Mounted Photovoltaic Modules and Systems," 2013.

[33] G. Heskestad, "Fire Plumes, Flame Height and Air Entrainment," in *SFPE Handbook of Fire Protection ENgineering*, 5th ed., M. J. Hurley, Ed. Springer, 2016, pp. 396–428.

[34] H. T. Loh and A. C. Fernandez-Pello, "Flow Assisted Flame Spread Over Thermally Thin Fuels," *Fire Safety Science*, vol. 1, pp. 65–74, 1986.

[35] G. H. Markstein and J. de Ris, "Upward fire spread over textiles," *Symposium (International) on Combustion*, vol. 14, no. 1, pp. 1085–1097, 1973.

[36] ISO, *ISO 5660-1: Reaction-to-fire tests — Heat release, smoke production and mass loss rate - Part 1: Heat release rate (cone calorimeter method)*. 2002.

[37] A. C. Fernandez-Pello and T. Hirano, "Controlling Mechanisms of Flame Spread," *Combustion Science and Technology*, vol. 32, no. 1–4, pp. 1–31, 1983.

[38] Bristish Standards Institution, *BS ISO 14934-4:2014 - Fire tests. Calibration and use of heat flux meters. Guidance on the use of heat flux meters in fire tests*. 2014.

[39] A. C. Fernandez-Pello and R. J. Santoro, "On the dominant mode of heat transfer in downward flame spread," *17th Symposium (International) on Combustion*, vol. 17, no. 1, pp. 1201–1209, 1979.

[40] A. Tewarson and S. D. Ogden, "Fire behavior of polymethylmethacrylate," *Combustion and Flame*, vol. 89, no. 3, pp. 237–259, 1992.

[41] J. Quintiere and M. T. Harkleroad, "New Concepts for Measuring Flame Spread Properties," *ASTM Special Technical Publication*, pp. 239–267, 1985.

[42] J. S. Kristensen, "Fire risk assessment of solar cell array installations on large buildings," Msc Thesis, Technical University of Denmark, 2015.

# APPENDIX 1: DETERMINING SAMPLE DIMENSIONS

Preliminary tests using sample of 300mm length and 300 mm was carried out with flame propagation and mass loss rate recorded. From the flame spread plots in Figure 44, there is an accelerating flame spread rate was observed for H = 15 cm, but more data points are required to obtain the overall trend. Thus, an extended slab of 700 mm was used for the final set-up in order to capture the overall general trend.

These preliminary studies are also intended to confirm the suitability of 300 mm width selection for the PMMA slab as there will be a splitting of flame front around the heat flux gauge that may affect the results. Based on mass readings plotted in Figure 45, the effect of flame splitting around the heat flux gauge have little impact on the mass loss rate. Similarly, there is no considerable disruption to the flame spread rate. Thus, 300 mm was deemed a suitable width for the tests.

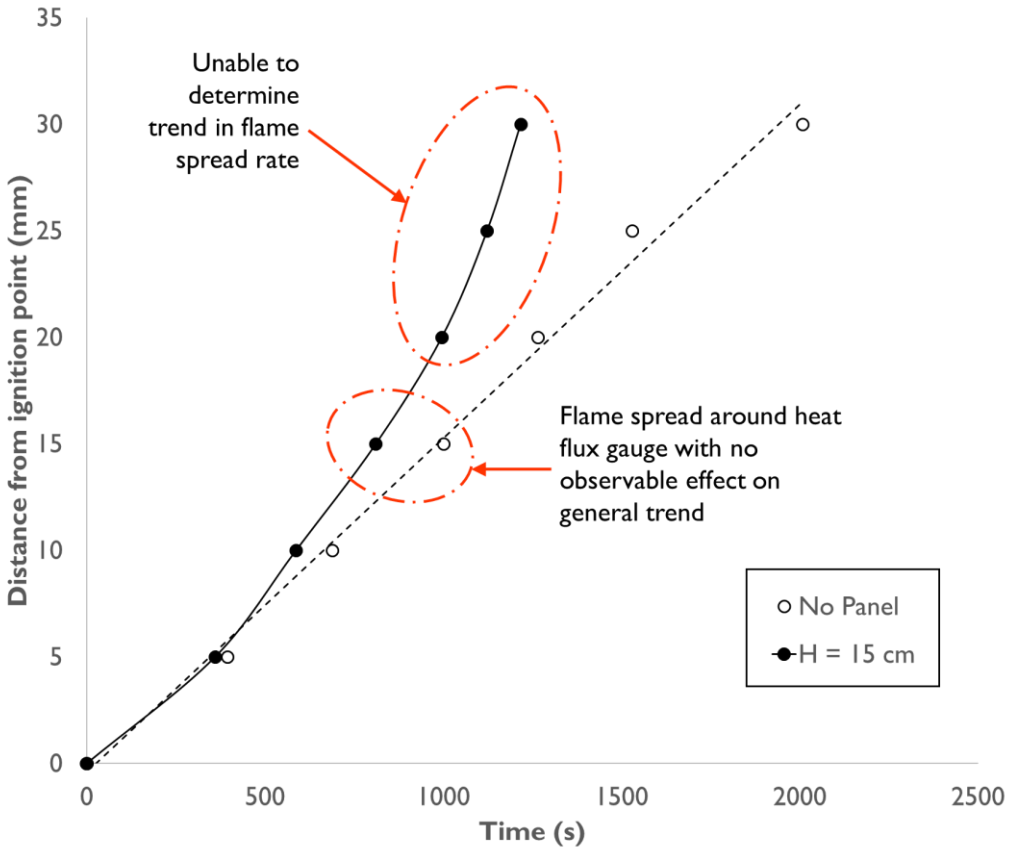


*Figure 44 Flame propagation over time for 300 mm length*

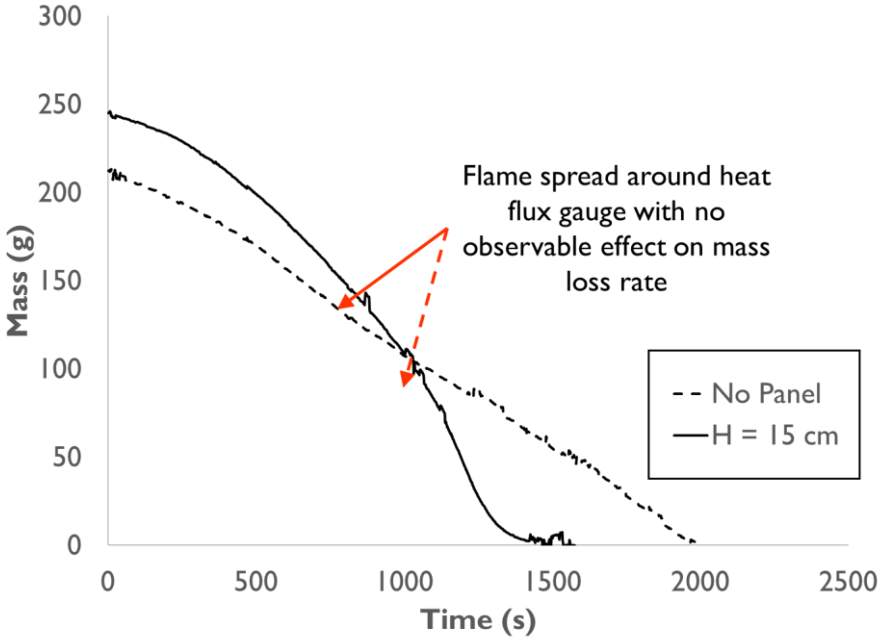


*Figure 45 Mass over time for 300 mm length*

# APPENDIX 2: FULL EXPERIMENTAL MATRIX

The following table shows the full experimental matrix that was carried out. These include the preliminary experiment done in order to ensure the final tests used for further analysis considers the identified issued in the preliminary tests.

| Test No. | Length of Sample (mm) | Panel Height, H (cm) | Comments |
|---|---|---|---|
| **1** | 300 | No Panel | The sample length was insufficient for full analysis. See Appendix 1. It was decided that a longer sample of 700 mm will be used for subsequent tests |
| **2** | 300 | 15 | |
| **3** | 700 | 15 | The PMMA sample was cut into two pieces using a knife with a straight line. However, the cut was not smooth and the joint could not be easily placed. It was decided to laser cut the PMMA sample into two pieces with a sawtooth cut in order to maintain good contact between the two pieces. |
| **4** | 700 | 15 | After the tests were carried out, it was observed that the mass loss from the experiments did not equate i.e. mass of sample seems to deviate considerably between tests. Investigations point to a mass balance scale gave drifting results. Subsequent tests were done with careful consideration of the changes in mass of the sample and set-up before and after the experiment. |
| **5** | 700 | 25 | |
| **6** | 700 | 15 | |
| **7** | 700 | 20 | These tests revealed that the flame spread is sensitive to draft. For subsequent test, it was ensured that the hood was fully closed on all sides |
| **8** | 700 | 20 | |
| **9** | 700 | 25 | |
| **10** | **700** | **No Panel** | **Shall be used for further analysis** |
| **11** | **700** | **25** | |
| **12** | **700** | **20** | |
| **13** | **700** | **17** | |
| **14** | **700** | **15** | |
| **15** | **700** | **10** | |
| **16** | **700** | **20 (Actual PV)** | |
| **17** | **700** | **17 (Actual PV)** | |
| **18** | **700** | **15 (Actual PV)** | |

# APPENDIX 3: PMMA TEMPERATURES (RAW DATA)

The temperature profile diagrams in Figure 29 were obtained based on the thermocouple readings for each test. The raw data used in the forming the temperature profiles for each test is shown in this Appendix.

**No Panel:**

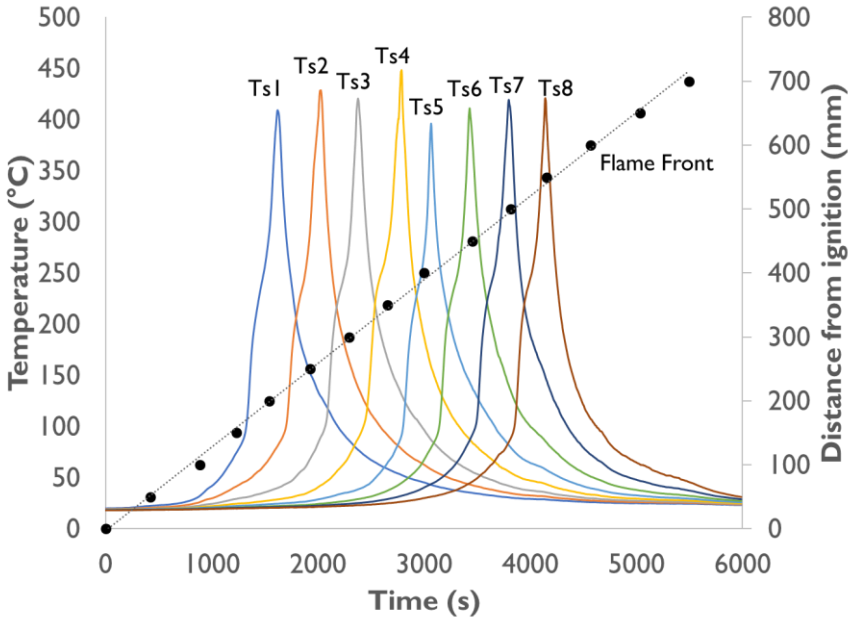


**H = 25 CM:**

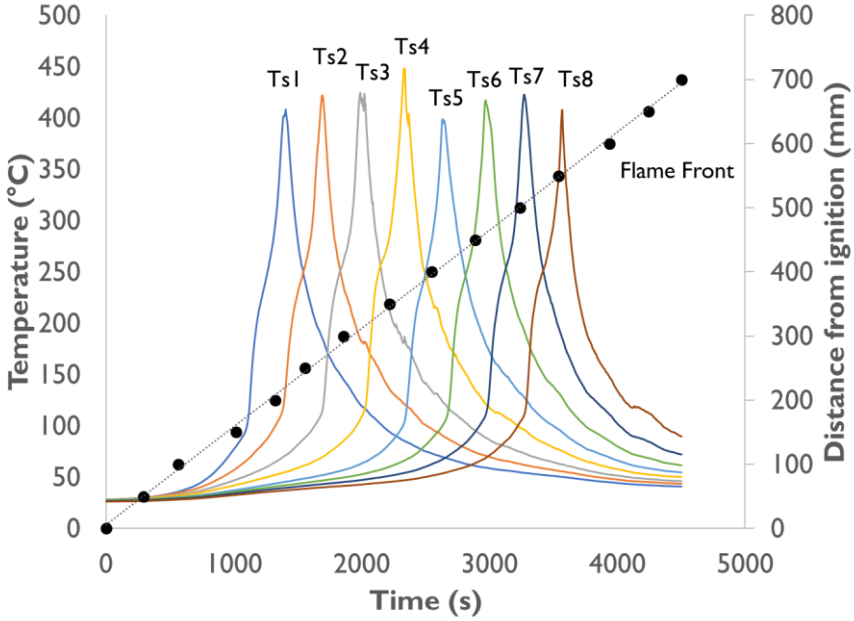

**H = 20 CM:**

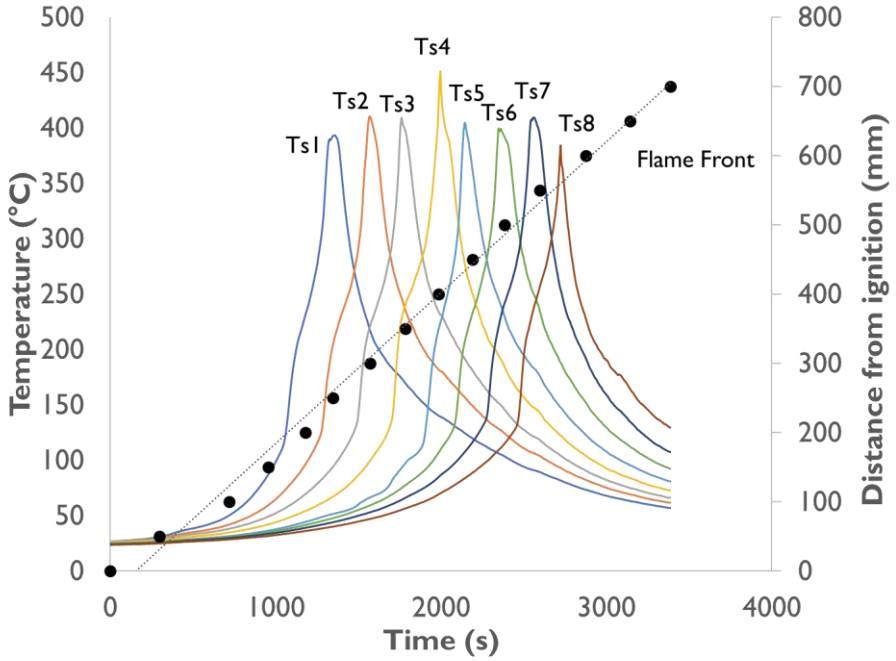
Ts1
Ts2
Ts3
Ts4
Ts5
Ts6
Ts7
Ts8
Flame Front
Temperature (°C)
Distance from ignition (mm)
Time (s)
0
50
100
150
200
250
300
350
400
450
500
0
100
200
300
400
500
600
700
800
0
1000
2000
3000
4000

**H = 17 CM**

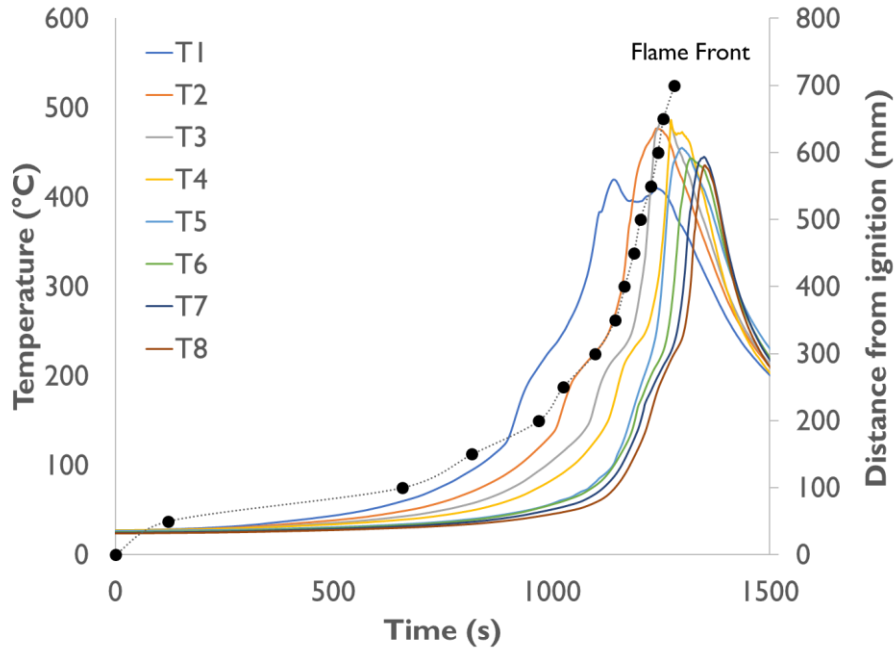
T1
T2
T3
T4
T5
T6
T7
T8
Flame Front
Temperature (°C)
Distance from ignition (mm)
Time (s)
0
100
200
300
400
500
600
0
100
200
300
400
500
600
700
800
0
500
1000
1500

**H = 15 CM:**

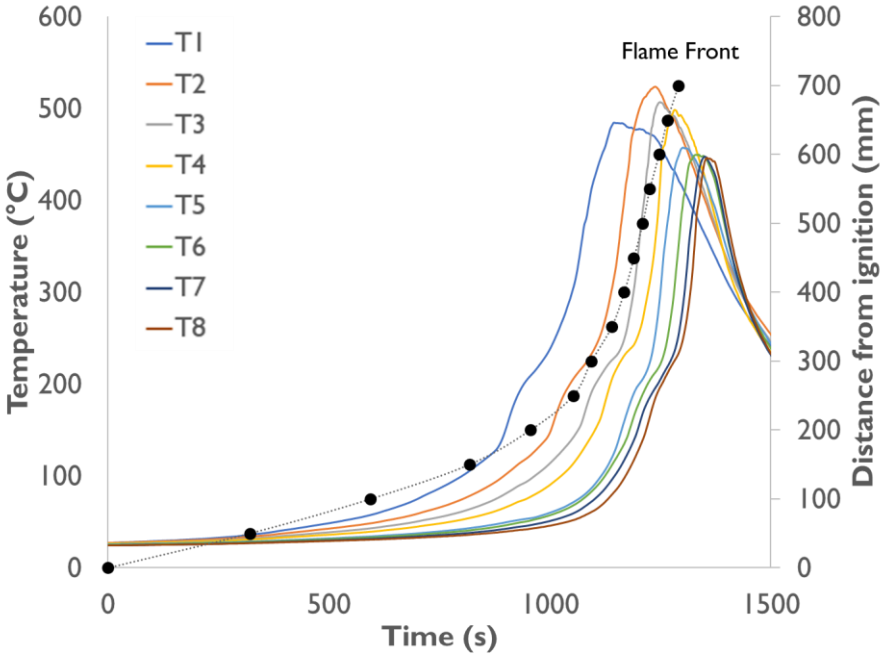
T1
T2
T3
T4
T5
T6
T7
T8
Flame Front
Temperature (°C)
Distance from ignition (mm)
Time (s)
0
100
200
300
400
500
600
700
800
0
500
1000
1500

**H = 10 CM:**

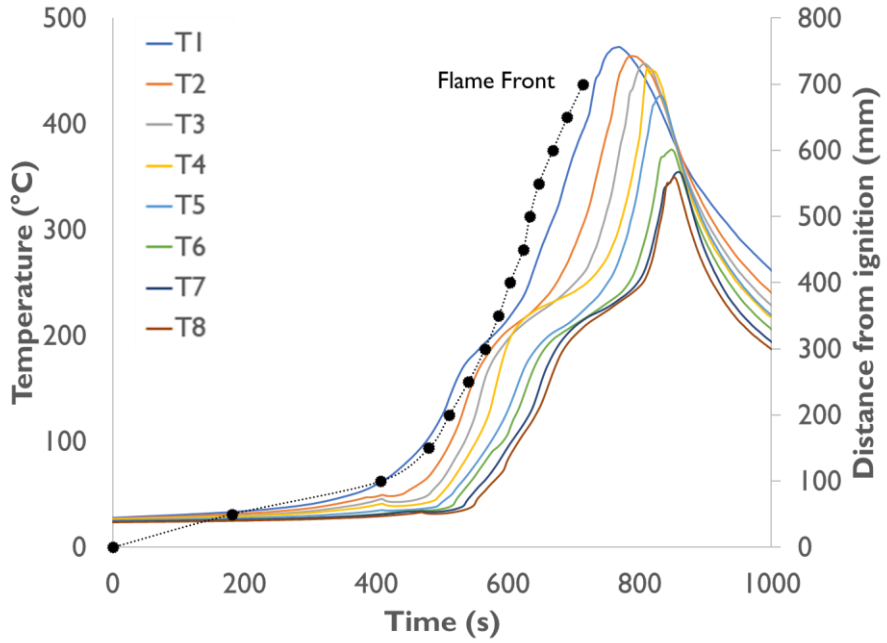
T1
T2
T3
T4
T5
T6
T7
T8
Flame Front
Temperature (°C)
Distance from ignition (mm)
Time (s)
0
100
200
300
400
500
600
700
800
0
200
400
600
800
1000

# APPENDIX 4: COMPARISON WITH PV PANELS

The experimental set-up with a surrogate panel and an actual PV panel shows similar results which would support the use of the surrogate panel for future work. Other than the results shown in the main paper, this section will show other measurement points to support the agreement between the surrogate panel and PV panels.

### Mass Loss Rate

Although there is a difference in the initial mass due to the variance in initial mass of the sample as explained in Section 3.3, the general trend is similar including the gradients of the graph which indicates mass loss rate. Deviation in the mass loss data for H = 17 cm is due to the difference in ignition fuel.

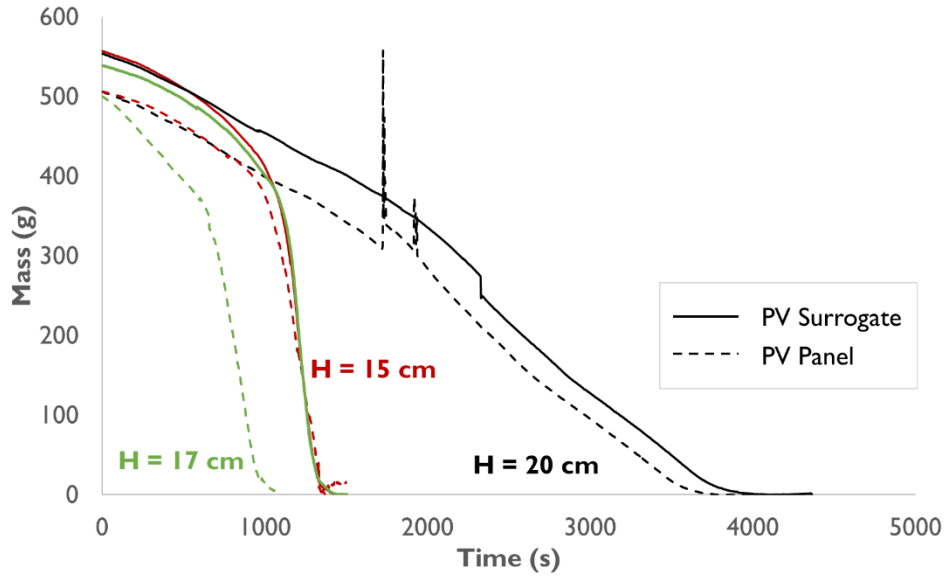


*Figure 46 Mass loss readings for PV surrogate and PV panel*

### Gas Temperatures

As the panel is not flat, gas temperature readings were modified as per Figure 38 in order to investigate whether there is an influence on the notch and the stagnation of hot gases within the notch. Based on the result from Figure 47, centreline temperatures are consistent with the temperature readings form the PV surrogate indicating that there is an agreement between both sets of tests. However, there is a significant lower temperature at the edge of the panel which is expected due to the ceiling jet formation. This difference also highlights the need for 3 dimensional studies to be conducted in order to be representative of real fires on roofs.

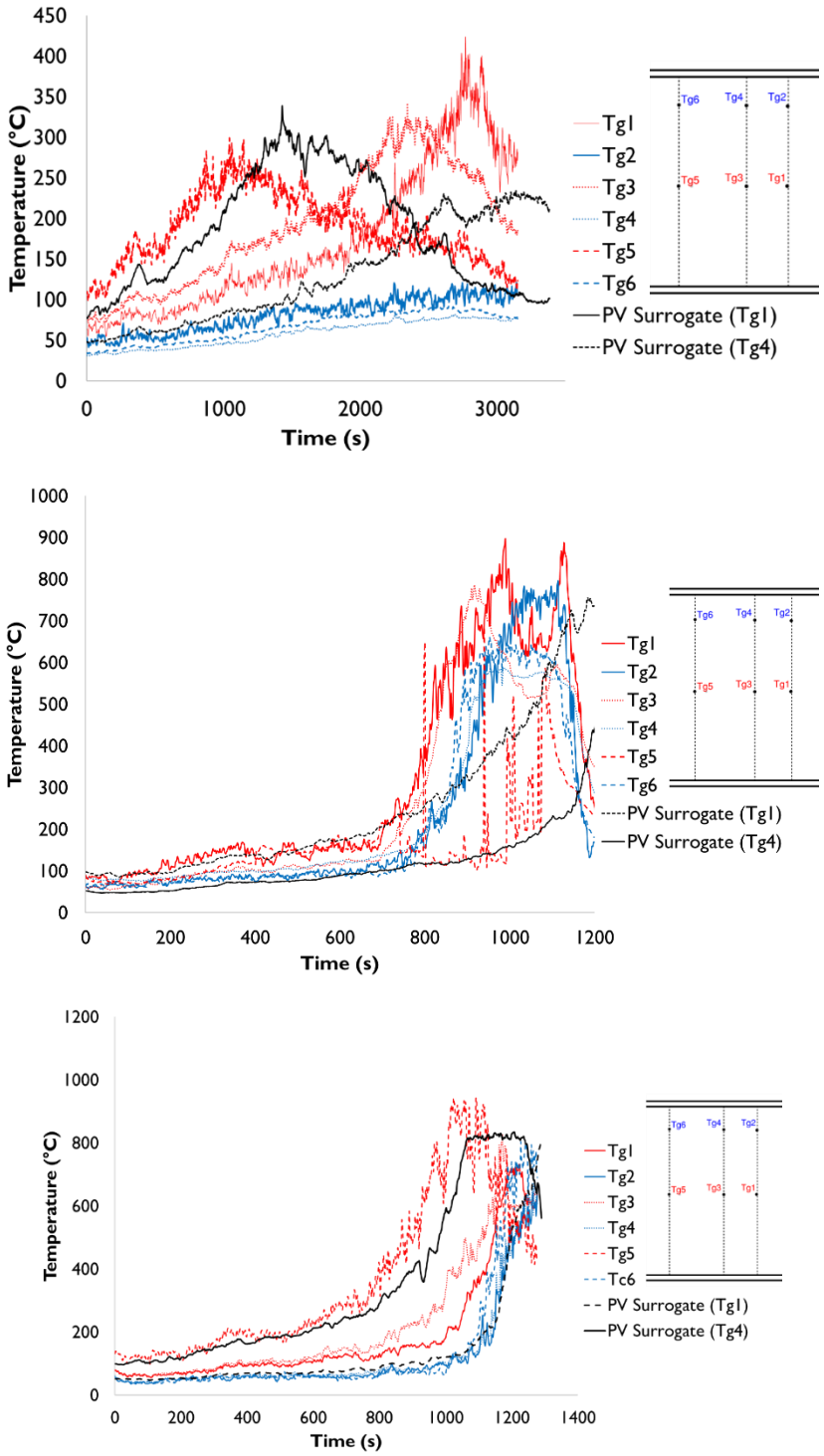


*Figure 47 Gas temperature comparison between PV surrogate and PV panel (top: H = 20 cm; middle: H = 17 cm; bottom: H = 15 cm)*

### Heat Flux Measurements

The radiative heat flux measurements also show close agreement although the readings for H = 17 cm and H = 15 cm were affected due to falling debris from the panel. This highlights the need to use a non-combustible surrogate such that measurements points are not affected

by the combustible materials. This is especially appropriate since the combustibility of the PV panel did not affect the fire spread behaviour. Thus, a surrogate PV material should be used.